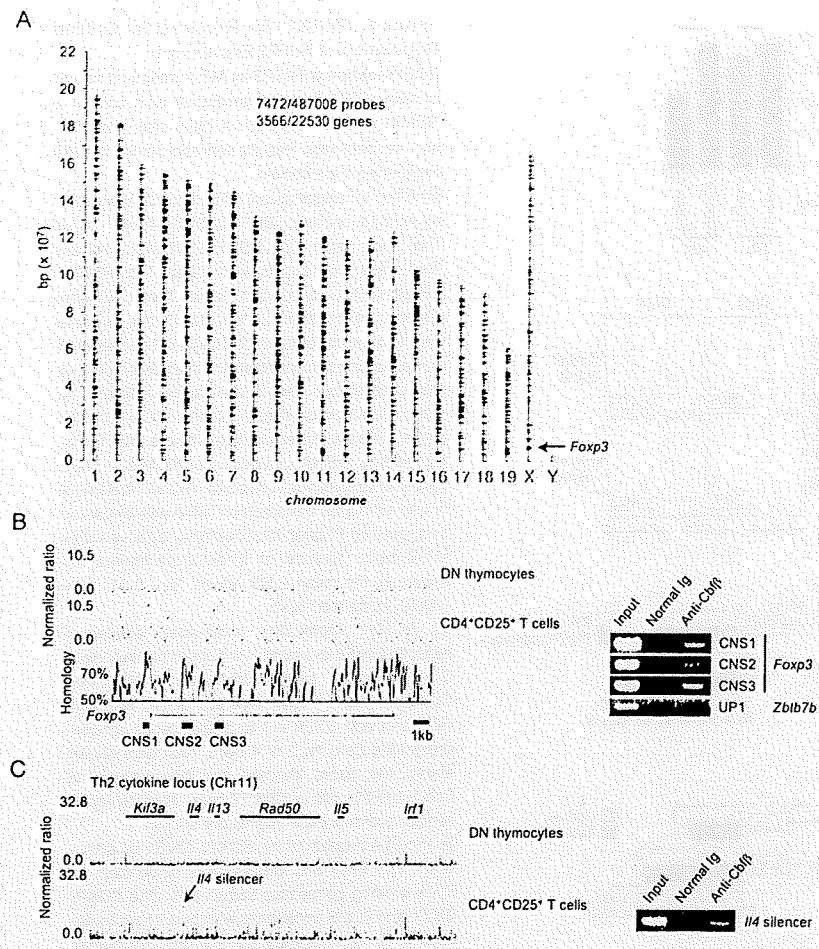

Figure 5. Binding of the Runx Complex to Regulatory Regions of *Foxp3* and *Il4*

(A) The Runx complex bound to promoter regions of various genes in Treg cells. MACS-purified $CD4^+CD25^+$ T cells of wild-type BALB/c mice were subjected to ChIP with anti-Cbfβ followed by promoter tiling array. Red crosses indicate Cbfβ-bound genes.

(B) The Runx complex bound to CNSs of the *Foxp3* gene in Treg cells of BALB/c mice. The binding of the Runx complex to the *Foxp3* gene locus in double negative (DN) thymocytes and peripheral $CD4^+CD25^-$ T cells from BALB/c mice was examined through a custom tiling array for the *Foxp3* locus coupled with ChIP with Cbfβ antibody (left). The signal intensity value of an individual probe is represented by a red dot in correspondence to the structure of the mouse *Foxp3* gene and mouse-human VISTA homology plot of the *Foxp3* gene. Red areas and blue areas in the VISTA plot indicate highly homologous regions and the exons of the mouse *Foxp3* gene, respectively. Gray squares in the figure of *Foxp3* gene structure indicate 5′ untranslated regions (UTRs). The binding of the Runx complex to CNSs of the *Foxp3* gene and the UP1 region of the *Zbtb7b* gene was assessed by conventional ChIP assays (right).

(C) The Runx complex bound to the *Il4* silencer in Treg cells of BALB/c mice. The binding of the Runx complex to the *Il4* silencer in $CD4^+CD25^+$ T cells from BALB/c mice was detected with the combination of ChIP and genome tiling array customized for Th2 cytokine locus (left) and conventional ChIP assays (right).

to the regulatory regions of *Foxp3*, *Il4*, and other genes in Treg cells.

RUNX1 Is Required for Optimal Regulation of FoxP3 Expression

The decreased FoxP3 expression in *Cbfb*-deleted Treg cells suggests that the Runx complex is required for constitutive FoxP3 expression in Treg cells. Because introduction of siRNA against *RUNX1* into human Treg cells efficiently repressed *RUNX1* expression (Ono et al., 2007), we examined the effect of *RUNX1* knockdown on FoxP3 expression in FoxP3-expressing T cell line MT-2 and in primary human $CD4^+CD25^{hi}$ cells. Both MT-2 cells and human Treg cells showed attenuated expression of FoxP3 after *RUNX1* siRNA transfection, indicating a key contribution of RUNX1 to the maintenance of constitutive FoxP3 expression (Figure 6A). Even in the presence of 100 U/ml of IL-2, Treg cells transduced with *RUNX1* siRNA still showed lower FoxP3 expression, indicating that attenuated FoxP3 expression was independent of IL-2 supply (Figure 6B). Further, by RT-PCR, *FOXP3* mRNA expression was slightly but significantly decreased in *Cbfb*-deleted Treg cells and *RUNX1* siRNA-introduced MT-2 cells, indicating that the Runx complex regulated FoxP3 expression, at least in part, at the level of transcription (Figure S6 and Figure 6C). Moreover, with human primary naive $CD4^+$ T cells, in which T cell receptor (TCR) stimulation can induce FoxP3 expression (Mantel et al., 2006; Walker et al., 2003), *RUNX1* knockdown attenuated this activation-induced FoxP3 expression (Figure 6D). This suggests that the Runx complex controls not only constitutive expression of FoxP3 in natural Treg cells but also its de novo induction in activated human $CD4^+$ T cells.

Given that the Runx complex binds to the possible regulatory regions of the *FOXP3* gene, it may directly control *FOXP3* transcription in Treg cells. We thus assessed the direct contribution of the Runx complex to *FOXP3* transcription by reporter gene assays. CNS1 and CNS3 of the human *FOXP3* gene exhibited significant transactivational activities in $CD4^+$ T cells (Figure S11A and Supplemental Data). The mutations of Runx-binding sites in the CNS1 and CNS3 constructs failed to attenuate the transactivational activities observed in those constructs (Figure S11B and Supplemental Data). However, the Runx-site mutations in CNS1 abrogated the transactivation of the construct in response to the stimulation (Figure 6E, left). In contrast to CNS1, the CNS3 construct, either of wild-type or mutant, showed no response to the stimulation (Figure 6E, right). Similar results were also observed in FoxP3-expressing ATL-43T, a human adult T cell leukemia cell line (Figure 6F).

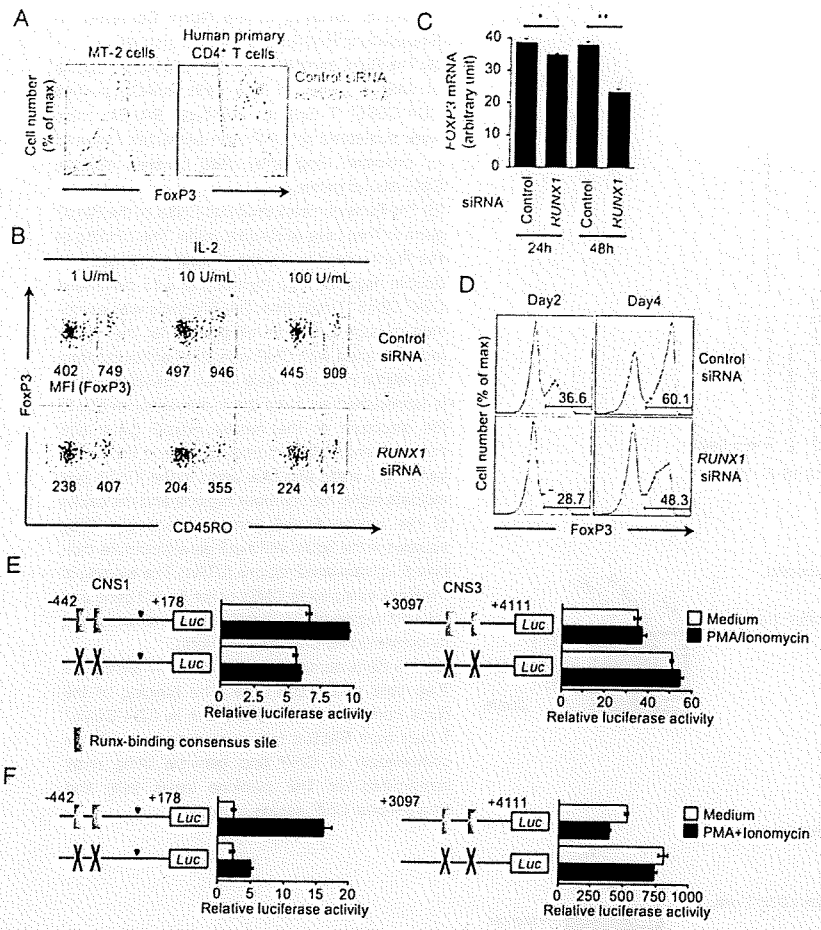

Figure 6. RUNX1 Was Required for Optimal Regulation of FoxP3 Expression

(A) Expression of FoxP3 by MT-2 cells and human primary CD4$^+$ T cells transduced with control or *RUNX1* siRNA 3 days and 4 days after transduction, respectively. Results representative of three experiments are shown.

(B) Effect of exogenous IL-2 on FoxP3 expression by human primary CD4$^+$CD25^{hi}CD45RO$^-$ naive Treg cells and CD4$^+$CD25^{hi}CD45RO$^+$ memory Treg cells transduced with control or *RUNX1* siRNA. siRNA-transduced human Treg cells were purified 24 hr after transduction; this process was followed by culture for 3 days in the presence of the indicated concentrations of exogenous IL-2. Numbers shown below the gates indicate the mean fluorescence intensity (MFI) of FoxP3 in the gates. Data are representative of two experiments.

(C) Relative mRNA expression of *FOXP3* in MT-2 cells transduced with control or *RUNX1* siRNA 24 hr and 48 hr after transduction. RNA was extracted from purified PI (propidium iodide)-negative viable MT-2 cells. Results of three experiments are shown as the mean ± SD values. $^*p = 0.01$; $^{**}p = 0.0001$ (unpaired t test).

(D) *RUNX1* knockdown attenuated activation-induced FoxP3 expression in human primary naive CD4$^+$ T cells. siRNA-introduced CD4$^+$CD25$^-$CD45RO$^-$ naive T cells were stimulated with anti-CD3 and anti-CD28 in the presence of antigen-presenting cells for 2 or 4 days. Numbers shown above the gates indicate the percentages of CD4$^+$FoxP3$^+$ cells in CD4$^+$ T cells. Results representative of two experiments are shown.

(E and F) Activation of the *FOXP3* CNS1 by stimulation with PMA and ionomycin is dependent on Runx-binding consensus sequences. The *FOXP3* CNS1 and CNS3 constructs with or without mutations in Runx sites were transfected into human primary CD4$^+$ T cells (E) and ATL 43T cells (F) and cultured in medium or in medium containing PMA and ionomycin. Results shown are the mean ± SD of triplicates done in one experiment representative of three.

Taken together, these results suggest that the Runx complex is required for optimal regulation of FoxP3 expression.

Analyses of *Runx1$^{F/F}$:FIC* and *Runx3$^{F/F}$:FIC* Mice

Because both Runx1 and Runx3 were expressed in Treg cells (Figure S12; Ono et al., 2007), we next investigated which one played a key role for Treg cell function in vivo. We generated *Runx1$^{F/F}$:FIC* and *Runx3$^{F/F}$:FIC* mice by crossing *FIC* mice with *Runx1*-floxed or *Runx3*-floxed mice, respectively (Naoe et al., 2007; Taniuchi et al., 2002). *Runx1$^{F/F}$:FIC* mice developed histologically evident gastritis, high titers of parietal cell antibodies, and hyperproduction of IgE as observed in *Cbfb$^{F/F}$:FIC* mice, whereas IgG production was not significantly altered (Figures 7A–7D). By contrast, *Runx3$^{F/F}$:FIC* mice did not develop gastritis, parietal cell antibodies, or hyperproduction of IgE (Figures 7B–7D). *Runx1*- but not *Runx3*-deleted Treg cells showed attenuated FoxP3 expression as observed in *Cbfb*-deleted Treg cells (Figure 7E). In addition, *Runx1*- or *Runx3*-deleted Treg cells did not lose CD103 expression, whereas *Cbfb*-deleted Treg cells lost it, indicating that Runx1 and Runx3 function redundantly in the regulation of CD103 expression (Figure 7F). Also, the finding indicates that autoimmune phenotypes due to Cbfβ deficiency in Treg cells is not attributed to the loss of CD103 expression because CD103 expression was not altered in autoimmune *Runx1$^{F/F}$:FIC* mice. Our results thus demonstrate that Runx1, but not Runx3, is indispensable for in vivo Treg cell function but do not exclude possible functional compensation between Runx1 and Runx3 in Treg cells.

DISCUSSION

In this study, we showed that Treg cell-specific deficiency of Cbfβ or Runx1, but not Runx3, impaired in vivo Treg cell function, resulting in the development of autoimmune disease and hyperproduction of IgE. The immunological diseases were similar in spectrum to those found in FoxP3 mutant or -deficient mice, although the disease severities were much milder (Sakaguchi et al., 2006).

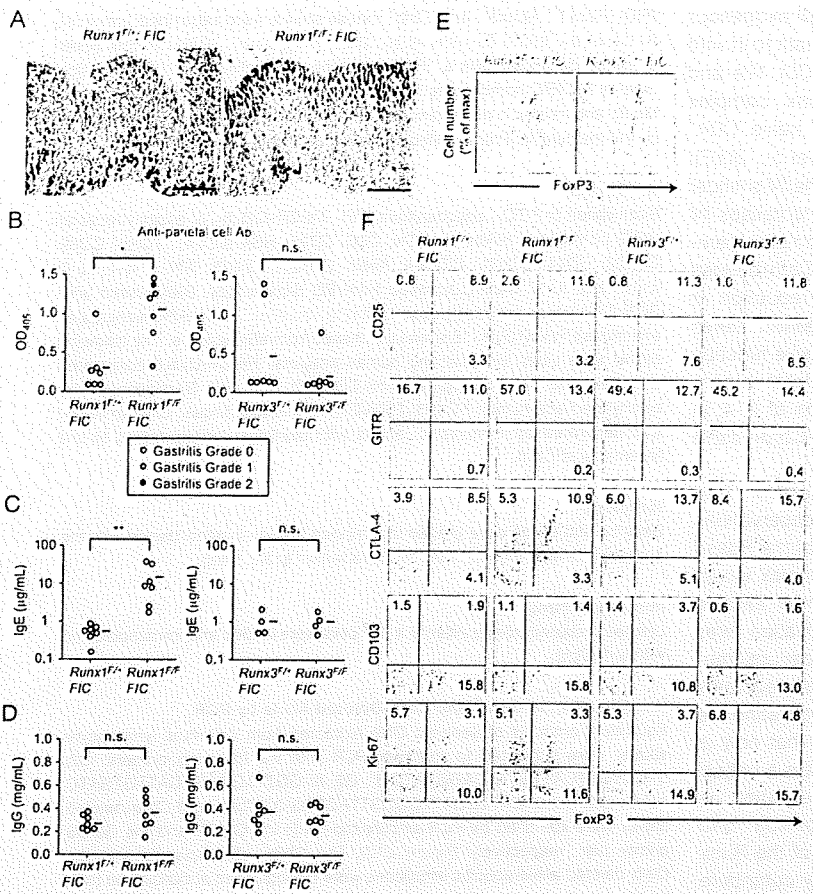

Figure 7. Development of Autoimmune Disease and Hyperproduction of IgE in *Runx1*$^{F/F}$*: FIC* Mice, but Not in *Runx3*$^{F/F}$*: FIC* Mice

(A) Hematoxylin and eosin staining of stomach sections of 8- to 9-week-old *Runx1*$^{F/F}$*: FIC* and *Runx1*$^{F/+}$*: FIC* littermates (n = 7). Representative photomicrographs are shown. Scale bars represent 10.0 μm.

(B) Titers of parietal cell autoantibodies in the sera of 8- to 9-week-old *Runx1*$^{F/F}$*: FIC* and *Runx1*$^{F/+}$*: FIC* littermates (n = 7) (left) and *Runx3*$^{F/F}$*: FIC* and *Runx3*$^{F/+}$*: FIC* littermates (n = 7) (right) were assessed by ELISA. Horizontal lines represent averages from each group. *p = 0.01.

(C and D) Titers of IgE (C) and IgG (D) in the sera of 8- to 9-week-old *Runx1*$^{F/F}$*: FIC* and *Runx1*$^{F/+}$*: FIC* littermates (n = 7) and *Runx3*$^{F/F}$*: FIC* and *Runx3*$^{F/+}$*: FIC* littermates (n = 4) were assessed by ELISA. Horizontal lines represent averages from each group. **p = 0.002.

(E) Flow cytometric analysis of FoxP3 expression by CD4$^+$ T cells from *Runx1*$^{F/F}$*: FIC* and *Runx1*$^{F/+}$*: FIC* littermates (left) and from *Runx3*$^{F/F}$*: FIC* and *Runx3*$^{F/+}$*: FIC* littermates (right) at 7 weeks of age. Results representative of three experiments are shown.

(F) Expression of FoxP3 and the indicated molecules by *Runx1*$^{F/F}$*: FIC* and *Runx1*$^{F/+}$*: FIC* littermates and by *Runx3*$^{F/F}$*: FIC* and *Runx3*$^{F/+}$*: FIC* littermates at 7 to 10 weeks of age. Results representative of three experiments are shown.

We have previously shown that Runx1 binds to the promoter of the *Il2* and *Ifng* genes and enhances IL-2 and IFN-γ production in conventional T cells. Conversely, the FoxP3-Runx1 complex, together with other transcription factors such as NFAT, represses the expression of these cytokines and confers in vitro-suppressive activity to Treg cells (Ono et al., 2007). Here, we have provided genetic evidence that Treg cell-specific deficiency of the Runx1-Cbfβ complex indeed impairs in vivo Treg cell function. This indicates that Runx-dependent gene regulation is critically required for in vivo Treg cell function. In addition, Cbfβ-deficient Treg cells transcribed *Il17a* and *Rorgt* to lesser extents than control Treg cells, whereas *Il4*, *Il10*, and *Tbx21* increased in the former. Other studies have shown that Runx1 induces the expression of RORγt, interacts with RORγt in conventional T cells, and regulates *Il17* transcription via controlling the promoter or enhancer regions of the *Il17* gene (Zhang et al., 2008). Runx3 also acts with T-bet to activate *Ifng* and silence *Il4* via binding to the *Ifng* promoter and the *Il4* silencer regions, respectively, leading to Th1 cell-specific cytokine production (Djuretic et al., 2007). Further, Runx1 and Runx3 interact with the *Cd4* silencer and the *Zbtb7b* silencer, in regulating thymocyte commitment to the CD8$^+$ T cell lineage by repressing the alternative cell fate (Setoguchi et al., 2008; Taniuchi et al., 2002). Thus, the Runx complex plays critical roles not only in T cell differentiation, in particular CD4-CD8 lineage commitment, but also in conferring a variety of functions to T cell subsets including Th1, Th17, and Treg cell. Further, phenotypical differences between *Runx1*- and *Runx3*-deleted Treg cells suggest that Runx1 and Runx3 differently contribute to the differentiation and the functions of T cell subsets. The Runx complex may thus function as an essential core transcriptional "modifier" to regulate specialized effector functions of CD4$^+$ T cell subsets by associating with particular lineage-specific transcription factors including FoxP3.

Regarding the mechanism by which Treg cell function is impaired in Cbfβ- or Runx1-deficient Treg cells, a notable finding is that Cbfβ or Runx1 deficiency accompanies attenuated expression of FoxP3 at mRNA and protein levels. Because attenuated FoxP3 expression can lead to loss of Treg cell-suppressive function, as demonstrated by others (Wan and Flavell, 2007), reduced expression of FoxP3 might be responsible for dysfunction of *Cbfb*-deleted Treg cells. For example, *Nrp1* and *Pde3b*, which were differentially expressed in *Cbfb*-deleted Treg cells by expression microarray, could be affected by FoxP3 hypoexpression. Other differentially expressed genes are also possibly associated with the impaired function of *Cbfb*-deleted Treg cells. They include *Il4*, *Ltb4r1*, *Cd160*, and *Ccr5*, all of which were overexpressed in *Cbfb*-deleted Treg cells. Of particular note is the hyperproduction of IL-4 by *Cbfb*-deleted Treg cells. Elevated IL-4 may contribute to the impaired Treg cell-mediated suppression in *Cbfb*- or *Runx1*-deleted Treg

cells because it has been shown that the addition of exogenous IL-4 renders $CD4^+CD25^-$ conventional T cells resistant to in vitro Treg cell-mediated suppression (Pace et al., 2006). We and others have previously reported that the Runx complex represses *Il4* via binding to the *Il4* silencer in naive $CD4^+$ T cells and Th1 cells (Djuretic et al., 2007; Nace et al., 2007). Our observation that the Runx complex bound to the *Il4* silencer in Treg cells suggests that the complex similarly represses *Il4* expression in Treg cells and that loss of Runx complex derepresses *Il4*, leading to hyperproduction of IL-4 in *Cbfb*-deleted Treg cells. Nonetheless, it is also possible that reduction of FoxP3 expression directly derepresses *Il4* expression. Taken together, our findings show that impaired suppressive function of *Cbfb*-deleted Treg cells could be attributed, at least in part, to the reduction of FoxP3 and the hyperproduction of IL-4, in addition to the impaired formation of the Runx-Cbfβ-FoxP3 complex (Ono et al., 2007).

The maintenance of constitutive FoxP3 expression in Treg cells appears to require the Runx complex. Our observations that the complex bound to the regulatory regions of the *Foxp3* gene in Treg cells may suggest that the Runx complex would directly upregulate FoxP3 expression. In the reporter assays, however, Runx-binding site-dependent transactivation was observed only under activated condition, and not under unstimulated condition. This suggests that the Runx complex regulates constitutive FoxP3 expression more than by transactivating the *FOXP3* gene. It has also been shown that RUNX1 not only is a conventional transcriptional activator but also plays a critical role in chromatin modifications such as histone acetylation via interacting with histone acetyltransferases (Yoshida and Kitabayashi, 2008). This suggests that the binding of the Runx complex to the *Foxp3* gene regulatory regions may contribute to constitutive FoxP3 expression through epigenetic regulation. It is also possible that the deficiency of the Runx complex may primarily dysregulate other genes encoding molecules necessary for the maintenance of FoxP3 expression in Treg cells. These possibilities are currently under investigation.

Our results support the concept that Runx-dependent program plays essential roles for immune homeostasis including Treg cell-mediated immune suppression. Single-nucleotide polymorphisms (SNPs) affecting the consensus sites for RUNX1 are associated with the genetic susceptibility to several autoimmune diseases including systemic lupus erythematosus, rheumatoid arthritis, and psoriasis (Alarcon-Riquelme, 2004; Helms et al., 2003; Prokunina et al., 2002; Tokuhiro et al., 2003). In addition, a SNP in the *RUNX1* gene itself was strongly associated with rheumatoid arthritis (Tokuhiro et al., 2003). It is thus likely that genetic alterations of *RUNX1* may contribute to the development of autoimmune diseases in part by means of affecting Treg cell-mediated immune regulation. Furthermore, our study suggests that Treg cell-specific inhibition of the activity of the Runx1-Cbfβ complex could be useful for reducing Treg cell activity and thereby evoking effective tumor immunity.

EXPERIMENTAL PROCEDURES

Mice

C.B-17 SCID mice were purchased from CLEA Japan (Tokyo, Japan). BALB/c mice were purchased from Japan SLC (Shizuoka, Japan). *Foxp3-Ires-Cre (FIC)*, *Runx1*^{F}, *Runx3*^{F}, and *Cbfb*^{F} mouse strains were described previously (Nace et al., 2007; Taniuchi et al., 2002; Wing et al., 2008). In this paper, a mouse described with a "*FIC*" genotype was either a *FIC/Y* hemizygote male or *FIC/FIC* homozygote female. All mice were maintained in our animal facility and treated in accordance with the guidelines for animal care approved by the Institute for Frontier Medical Sciences, Kyoto University.

Antibodies

Biotinylated or FITC-, phycoerythrin (PE)-, PerCP-Cy5.5-, or allophycocyanin (APC)-conjugated mAbs for CD4, CD8, CD25, HSA (CD24), TCRβ, CD69, CD122, CD44, CD62L, CTLA-4, Ki-67, CD127, CD103, IFN-γ, IL-2, IL-4, IL-10, and IL-17 were purchased from BD Biosciences. Biotinylated anti-GITR (DTA1) was previously described (Shimizu et al., 2002). APC-conjugated anti-mouse Foxp3 (FJK-16 s) was purchased from eBioscience. The following mAbs were used for detecting human antigens: PerCP-Cy5.5-conjugated anti-CD4 and FITC-conjugated anti-CD45RO from BD Biosciences and biotinylated anti-human FOXP3 (236A/E7) from eBiosciences. Cbfβ antibody was generated by immunizing rabbits with peptides corresponding to the N-terminal of Cbfβ.

Histology

Gastritis and colitis were graded in a blinded fashion in accordance with the published criteria (Asano et al., 1996; Asseman et al., 1999).

Immunoblotting

Lysates prepared from purified 5×10^3 cells were loaded and immunoblotted with anti-Cbfβ.

Identification of *Cbfb*^{F} and *Cbfb*-Deleted Allele by PCR

Equivalent amounts of genomic DNA extracted from individual lymphocyte subset were subjected to multiplex PCR with the following primers: G2, 5′-CCTCCTCATTCTAACAGGAATC-3′; G3, 5′-GGTTAGGAGTCATTGTGATC AC-3′; and G6, 5′-CATTGGATTGGCGTTACTGG-3′. *Cbfb*^{F} and *Cbfb*-deleted alleles were identified by PCR amplification with the G3/G2 and the G3/G6 primer pair, respectively (Figure S13). The *Cbfb*^{F} allele-specific and the *Cbfb*-deleted allele-specific amplicons were distinguished according to their length.

ELISA

Autoantibodies specific for gastric parietal cells were detected by ELISA as previously described (Sakaguchi et al., 1995). Serum IgG and IgE levels were assessed by ELISA with Mouse IgG ELISA Quantitation Kit (Bethyl Laboratories) and OptEIA Mouse IgE ELISA set (BD Biosciences), respectively.

Cell Sorting

Fresh mouse $CD4^+$ T cells were isolated as previously described (Hori et al., 2003). Then, $CD4^+$ T cell subpopulations including $CD4^+CD25^{hi}$ cells, $CD4^+CD25^-$ cells, and $CD4^+CD25^-CD45RB^{hi}$ cells were purified by sorting with a cell sorter (MoFlo, Dako). In some experiments, $CD4^+CD25^+$ cells were purified by MACS (Miltenyi Biotec).

Intracellular Cytokine Staining

Cells were stimulated for 5 hr with 20 ng/ml phorbol 12-myristate 13-acetate (PMA) and 1 μM ionomycin in the presence of GolgiStop (BD Biosciences). For intracellular cytokine staining, stimulated cells were stained for surface antigens, fixed, permeabilized with BD Cytofix/Cytoperm (BD Biosciences), and stained by anti-cytokine. For costaining of intracellular cytokine and FoxP3, stimulated cells were stained for surface antigens, fixed, permeabilized with Foxp3 Fixation/Permeabilization Kit (eBioscience), and finally, costained with cytokine antibody and Foxp3 antibody.

Proliferation Assay and Suppression Assay

A total of 2×10^4 responder T cells were cultured with or without graded numbers of suppressor cells for 3 days in the presence of 4×10^4 antigen-presenting cells (mitomycin C-treated $Thy1.2^+$ cell-depleted BALB/c splenocytes) and 0.5 μg/ml CD3 antibody (145-2C11, BD Biosciences). [^{3}H]thymidine (1 μCi/well) was added during the last 8 hr of culture.

Quantitative Real-Time RT-PCR

Total RNA was prepared from cells of interest with RNeasy Mini Kit (QIAGEN). cDNA was synthesized from total RNA with SuperScript III reverse transcriptase and oligo$(dT)_{12-18}$ primer (Invitrogen). Quantitative real-time RT-PCR was performed with the LightCycler 480 System (Roche Applied Science) with QuantiTect SYBR Green PCR Kit (QIAGEN). Primer pairs used are listed in Table S4. All samples were run in triplicate and the data were normalized to *Hprt* mRNA expression.

Chromatin Immunoprecipitation and Tiling Array

Cells were crosslinked by the addition of one-tenth volume of fresh 11% formaldehyde solution for 10 min at room temperature. Cells were resuspended, lysed in lysis buffers, and sonicated for solubilization and shearing of crosslinked DNA. The cell extract was incubated overnight at 4 C with 100 μl of Dynal anti-rabbit IgG magnetic beads that had been preincubated with 10 μg of the Cbfβ antibody. Beads were washed five times with RIPA buffer and one time with TE containing 50 mM NaCl. Bound complexes were eluted from the beads by heating at 65 C with occasional vortexing, and crosslinking was reversed by overnight incubation at 65 C. Immunoprecipitated DNA and whole-cell extract DNA were then purified by treatment with RNaseA, proteinase K, and multiple phenol:chloroform:isoamyl alcohol extractions. For conventional ChIP assays, the precipitated DNA was subjected to PCR amplification. The primers used are as follows: FxCNS1-for, 5′-AGCCCTGT TATCTCATTGATAC-3′; FxCNS1-rev, 5′-GACCTCGCTCTTCTAATAATCC-3′; FxCNS2-for, 5′-CCCATACCCACACTTTTGACCTCTG-3′; FxCNS2-rev, 5′-GC ACTTGAAAATGAGATAACTGTTCA-3′; FxCNS3-for, 5′-CTGGCATCCAAGAA AGACA-3′; and FxCNS3-rev, 5′-GGCTTCATCGGCAACAA-3′. Primers for *Il4* silencer region and for the region at 1 kb upstream of *Zbtb7b* (*Th-POK*) exon Ia (UP1) were described previously (Naoe et al., 2007; Setoguchi et al., 2008). For a ChIP-on-chip experiment, purified DNA was amplified twice by LM-PCR in accordance with the manufacturer's protocol (Agilent). We used mouse promoter array and custom microarrays generated by Agilent that tiled through several loci via 60-nucleotide oligonucleotide probes. The probes, representing the forward strand, were spaced every 200 bases and were printed at random location on the array. Probe hybridization and scanning of oligonucleotide array data were performed in accordance with the manufacturer's protocol (Agilent). Data analyses were carried out with Feature Extraction software and ChIP Analytics software (Agilent).

RNA Interference

MT-2 cells and MACS-sorted primary human $CD4^+$ T cells were transduced with *RUNX1* siRNA (HSS141472; Invitrogen) or Stealth RNAi negative control GC high (Invitrogen) as previously described (Ono et al., 2007).

Expression Microarray

Total RNA was isolated with the RNeasy Micro Kit (QIAGEN). Biotinylated antisense cRNA was prepared by two cycles of in vitro amplication. Biotinylated cRNA (15 μg) was hybridized to Affymetrix GeneChip Mouse Genome 430 2.0 arrays. Data analyses were done with the use of MeV (v4.2) (Saeed et al., 2003).

Induction of FoxP3 Expression in Human Naive T Cells

$CD25^-CD45RO^-$ primary human naive T cells were negatively sorted with MACS Pan T Cell Isolation Kit II, CD25 MicroBeads, and CD45RO MicroBeads (Miltenyi Biotec). A total of 7×10^6 purified naive T cells were transduced with control or *RUNX1* siRNA with a Human T Cell Nucleofector Kit (Amaxa), mixed with 4×10^6 T cell-depleted syngeneic PBMCs, and then cultured in a volume of 1 ml (12-well plates) for 24 h. Then, 7×10^5 cells were harvested and cultured in a volume of 200 μl (96-well plates) in the presence of 0.01 μg/ml anti-CD3 (OKT3) and 0.02 μg/ml anti-CD28 (CD28.2) for 4 days. Blood samples were obtained from healthy adult volunteers (20–40 years old). The study was conducted with the approval from the human ethics committee of the Institute for Frontier Medical Sciences, Kyoto University.

Statistical analysis

Comparisons were analyzed for statistical significance by Mann-Whitney U test, unless otherwise stated, with $p < 0.05$ being considered significant.

ACCESSION NUMBERS

Microarray data are available from the National Center for Biotechnology Information Gene Expression Omnibus (GEO) under accession number GSE18148.

SUPPLEMENTAL DATA

Supplemental Data include 13 figures, 5 tables, and Supplemental Experimental Procedures and can be found with this article online at http://www.cell.com/immunity/supplemental/S1074-7613(09)00407-5.

ACKNOWLEDGMENTS

We thank M. Kakino, R. Ishii, M. Yoshida, and K. Akiyama for technical assistance; M. Matsuoka for ATL-43T cell line; and M. Matsushita for preparing histology.

Received: August 24, 2009
Revised: September 9, 2009
Accepted: September 14, 2009
Published online: October 1, 2009

REFERENCES

Alarcon-Riquelme, M.E. (2004). Role of RUNX in autoimmune diseases linking rheumatoid arthritis, psoriasis and lupus. Arthritis Res. Ther. *6*, 169–173.

Annacker, O., Coombes, J.L., Malmstrom, V., Uhlig, H.H., Bourne, T., Johansson-Lindbom, B., Agace, W.W., Parker, C.M., and Powrie, F. (2005). Essential role for CD103 in the T cell-mediated regulation of experimental colitis. J. Exp. Med. *202*, 1051–1061.

Asano, M., Toda, M., Sakaguchi, N., and Sakaguchi, S. (1996). Autoimmune disease as a consequence of developmental abnormality of a T cell subpopulation. J. Exp. Med. *184*, 387–396.

Asseman, C., Mauze, S., Leach, M.W., Coffman, R.L., and Powrie, F. (1999). An essential role for interleukin 10 in the function of regulatory T cells that inhibit intestinal inflammation. J. Exp. Med. *190*, 995–1004.

Bettelli, E., Dastrange, M., and Oukka, M. (2005). Foxp3 interacts with nuclear factor of activated T cells and NF-kappa B to repress cytokine gene expression and effector functions of T helper cells. Proc. Natl. Acad. Sci. USA *102*, 5138–5143.

Cao, X., Cai, S.F., Fehniger, T.A., Song, J., Collins, L.I., Piwnica-Worms, D.R., and Ley, T.J. (2007). Granzyme B and perforin are important for regulatory T cell-mediated suppression of tumor clearance. Immunity *27*, 635–646.

de Bruijn, M.F., and Speck, N.A. (2004). Core-binding factors in hematopoiesis and immune function. Oncogene *23*, 4238–4248.

Djuretic, I.M., Levanon, D., Negreanu, V., Groner, Y., Rao, A., and Ansel, K.M. (2007). Transcription factors T-bet and Runx3 cooperate to activate Ifng and silence Il4 in T helper type 1 cells. Nat. Immunol. *8*, 145–153.

Durst, K.L., and Hiebert, S.W. (2004). Role of RUNX family members in transcriptional repression and gene silencing. Oncogene *23*, 4220–4224.

Egawa, T., Tillman, R.E., Naoe, Y., Taniuchi, I., and Littman, D.R. (2007). The role of the Runx transcription factors in thymocyte differentiation and in homeostasis of naive T cells. J. Exp. Med. *204*, 1945–1957.

Fontenot, J.D., Gavin, M.A., and Rudensky, A.Y. (2003). Foxp3 programs the development and function of CD4+CD25+ regulatory T cells. Nat. Immunol. *4*, 330–336.

Gondek, D.C., Lu, L.F., Quezada, S.A., Sakaguchi, S., and Noelle, R.J. (2005). Cutting edge: Contact-mediated suppression by CD4+CD25+ regulatory cells involves a granzyme B-dependent, perforin-independent mechanism. J. Immunol. *174*, 1783–1786.

Grueter, B., Petter, M., Egawa, T., Laule-Kilian, K., Aldrian, C.J., Wuerch, A., Ludwig, Y., Fukuyama, H., Wardemann, H., Waldschuetz, R., et al. (2005). Runx3 regulates integrin alpha E/CD103 and CD4 expression during development of CD4-/CD8+ T cells. J. Immunol. *175*, 1694–1705.

Helms, C., Cao, L., Krueger, J.G., Wijsman, E.M., Chamian, F., Gordon, D., Heffernan, M., Daw, J.A., Robarge, J., Ott, J., et al. (2003). A putative RUNX1 binding site variant between SLC9A3R1 and NAT9 is associated with susceptibility to psoriasis. Nat. Genet. *35*, 349–356.

Hill, J.A., Feuerer, M., Tash, K., Haxhinasto, S., Perez, J., Melamed, R., Mathis, D., and Benoist, C. (2007). Foxp3 transcription-factor-dependent and -independent regulation of the regulatory T cell transcriptional signature. Immunity *27*, 786–800.

Hori, S., Nomura, T., and Sakaguchi, S. (2003). Control of regulatory T cell development by the transcription factor Foxp3. Science *299*, 1057–1061.

Khattri, R., Cox, T., Yasayko, S.A., and Ramsdell, F. (2003). An essential role for Scurfin in CD4+CD25+ T regulatory cells. Nat. Immunol. *4*, 337–342.

Kim, H.P., and Leonard, W.J. (2007). CREB/ATF-dependent T cell receptor-induced FoxP3 gene expression: A role for DNA methylation. J. Exp. Med. *204*, 1543–1551.

Komine, O., Hayashi, K., Natsume, W., Watanabe, T., Seki, Y., Seki, N., Yagi, R., Sukzuki, W., Tamauchi, H., Hozumi, K., et al. (2003). The Runx1 transcription factor inhibits the differentiation of naive CD4+ T cells into the Th2 lineage by repressing GATA3 expression. J. Exp. Med. *198*, 51–61.

Li, B., Samanta, A., Song, X., Iacono, K.T., Bembas, K., Tao, R., Basu, S., Riley, J.L., Hancock, W.W., Shen, Y., et al. (2007). FOXP3 interactions with histone acetyltransferase and class II histone deacetylases are required for repression. Proc. Natl. Acad. Sci. USA *104*, 4571–4576.

Mantel, P.Y., Ouaked, N., Ruckert, B., Karagiannidis, C., Welz, R., Blaser, K., and Schmidt-Weber, C.B. (2006). Molecular mechanisms underlying FOXP3 induction in human T cells. J. Immunol. *176*, 3593–3602.

Naoe, Y., Setoguchi, R., Akiyama, K., Muroi, S., Kuroda, M., Hatam, F., Littman, D.R., and Taniuchi, I. (2007). Repression of interleukin-4 in T helper type 1 cells by Runx/Cbf beta binding to the Il4 silencer. J. Exp. Med. *204*, 1749–1755.

Ochs, H.D., Ziegler, S.F., and Torgerson, T.R. (2005). FOXP3 acts as a rheostat of the immune response. Immunol. Rev. *203*, 156–164.

Ono, M., Yaguchi, H., Ohkura, N., Kitabayashi, I., Nagamura, Y., Nomura, T., Miyachi, Y., Tsukada, T., and Sakaguchi, S. (2007). Foxp3 controls regulatory T-cell function by interacting with AML1/Runx1. Nature *446*, 685–689.

Pace, L., Rizzo, S., Palombi, C., Brombacher, F., and Doria, G. (2006). Cutting edge: IL-4-induced protection of CD4+CD25- Th cells from CD4+CD25+ regulatory T cell-mediated suppression. J. Immunol. *176*, 3900–3904.

Prokunina, L., Castillejo-Lopez, C., Oberg, F., Gunnarsson, I., Berg, L., Magnusson, V., Brookes, A.J., Tentler, D., Kristjansdottir, H., Grondal, G., et al. (2002). A regulatory polymorphism in PDCD1 is associated with susceptibility to systemic lupus erythematosus in humans. Nat. Genet. *32*, 666–669.

Saeed, A.I., Sharov, V., White, J., Li, J., Liang, W., Bhagabati, N., Braisted, J., Klapa, M., Currier, T., Thiagarajan, M., et al. (2003). TM4: A free, open-source system for microarray data management and analysis. Biotechniques *34*, 374–378.

Sakaguchi, S., Ono, M., Setoguchi, R., Yagi, H., Hori, S., Fehervari, Z., Shimizu, J., Takahashi, T., and Nomura, T. (2006). Foxp3+ CD25+ CD4+ natural regulatory T cells in dominant self-tolerance and autoimmune disease. Immunol. Rev. *212*, 8–27.

Sakaguchi, S., Sakaguchi, N., Asano, M., Itoh, M., and Toda, M. (1995). Immunologic self-tolerance maintained by activated T cells expressing IL-2 receptor alpha-chains (CD25). Breakdown of a single mechanism of self-tolerance causes various autoimmune diseases. J. Immunol. *155*, 1151–1164.

Sato, T., Ohno, S., Hayashi, T., Sato, C., Kohu, K., Satake, M., and Habu, S. (2005). Dual functions of Runx proteins for reactivating CD8 and silencing CD4 at the commitment process into CD8 thymocytes. Immunity *22*, 317–328.

Setoguchi, R., Tachibana, M., Naoe, Y., Muroi, S., Akiyama, K., Tezuka, C., Okuda, T., and Taniuchi, I. (2008). Repression of the transcription factor Th-POK by Runx complexes in cytotoxic T cell development. Science *319*, 822–825.

Shimizu, J., Yamazaki, S., Takahashi, T., Ishida, Y., and Sakaguchi, S. (2002). Stimulation of CD25(+)CD4(+) regulatory T cells through GITR breaks immunological self-tolerance. Nat. Immunol. *3*, 135–142.

Speck, N.A. (2001). Core binding factor and its role in normal hematopoietic development. Curr. Opin. Hematol. *8*, 192–196.

Taniuchi, I., and Littman, D.R. (2004). Epigenetic gene silencing by Runx proteins. Oncogene *23*, 4341–4345.

Taniuchi, I., Osato, M., Egawa, T., Sunshine, M.J., Bae, S.C., Komori, T., Ito, Y., and Littman, D.R. (2002). Differential requirements for Runx proteins in CD4 repression and epigenetic silencing during T lymphocyte development. Cell *111*, 621–633.

Tokuhiro, S., Yamada, R., Chang, X., Suzuki, A., Kochi, Y., Sawada, T., Suzuki, M., Nagasaki, M., Ohtsuki, M., Ono, M., et al. (2003). An intronic SNP in a RUNX1 binding site of SLC22A4, encoding an organic cation transporter, is associated with rheumatoid arthritis. Nat. Genet. *35*, 341–348.

Tone, Y., Furuuchi, K., Kojima, Y., Tykocinski, M.L., Greene, M.I., and Tone, M. (2008). Smad3 and NFAT cooperate to induce Foxp3 expression through its enhancer. Nat. Immunol. *9*, 194–202.

van Wijnen, A.J., Stein, G.S., Gergen, J.P., Groner, Y., Hiebert, S.W., Ito, Y., Liu, P., Neil, J.C., Ohki, M., and Speck, N. (2004). Nomenclature for Runt-related (RUNX) proteins. Oncogene *23*, 4209–4210.

Walker, M.R., Kasprowicz, D.J., Gersuk, V.H., Benard, A., Van Landeghen, M., Buckner, J.H., and Ziegler, S.F. (2003). Induction of FoxP3 and acquisition of T regulatory activity by stimulated human CD4+CD25- T cells. J. Clin. Invest. *112*, 1437–1443.

Wan, Y.Y., and Flavell, R.A. (2007). Regulatory T-cell functions are subverted and converted owing to attenuated Foxp3 expression. Nature *445*, 766–770.

Wing, K., Onishi, Y., Prieto-Martin, P., Yamaguchi, T., Miyara, M., Fehervari, Z., Nomura, T., and Sakaguchi, S. (2008). CTLA-4 control over Foxp3+ regulatory T cell function. Science *322*, 271–275.

Woolf, E., Xiao, C., Fainaru, O., Lotem, J., Rosen, D., Negreanu, V., Bernstein, Y., Goldenberg, D., Brenner, O., Berke, G., et al. (2003). Runx3 and Runx1 are required for CD8 T cell development during thymopoiesis. Proc. Natl. Acad. Sci. USA *100*, 7731–7736.

Wu, Y., Borde, M., Heissmeyer, V., Feuerer, M., Lapan, A.D., Stroud, J.C., Bates, D.L., Guo, L., Han, A., Ziegler, S.F., et al. (2006). FOXP3 controls regulatory T cell function through cooperation with NFAT. Cell *126*, 375–387.

Yoshida, H., and Kitabayashi, I. (2008). Chromatin regulation by AML1 complex. Int. J. Hematol. *87*, 19–24.

Zhang, F., Meng, G., and Strober, W. (2008). Interactions among the transcription factors Runx1, RORgammat and Foxp3 regulate the differentiation of interleukin 17-producing T cells. Nat. Immunol. *9*, 1297–1306.

Developmental Biology 329 (2009) 176–190

Contents lists available at ScienceDirect

Developmental Biology

journal homepage: www.elsevier.com/developmentalbiology

Brpf1, a subunit of the MOZ histone acetyl transferase complex, maintains expression of anterior and posterior *Hox* genes for proper patterning of craniofacial and caudal skeletons

Kenta Hibiya [a], Takuo Katsumoto [b], Takashi Kondo [c], Issay Kitabayashi [b], Akira Kudo [a,*]

[a] Department of Biological Information, Tokyo Institute of Technology, 4259-B-32 Nagatsuta-cho, Midori-ku, Yokohama 226-8501, Japan
[b] Molecular Oncology Division, National Cancer Center Research Institute, 5-1-1 Tsukiji, Chuo-ku, Tokyo, 104-0045, Japan
[c] Kondo Research Unit, Neuro-Developmental Disorder Research Group, Brain Science Institute, Institute of Physical and Chemical Research (RIKEN), 2-1 Hirosawa, Wako, Saitama 351-0198, Japan

ARTICLE INFO

Article history:
Received for publication 10 October 2008
Revised 22 January 2009
Accepted 18 February 2009
Available online 27 February 2009

Keywords:
Brpf1
Moz
TrxG
Medaka
Mutant
bis
Hox
Skeleton
Fin ray

ABSTRACT

The epigenetic mechanism involving chromatin modification plays a critical role in the maintenance of the expression of *Hox* genes. Here, we characterize a mutant of the medaka fish, named *biaxial symmetries* (*bis*), in which *brpf1*, a subunit of the MOZ histone acetyl transferase (HAT) complex, is mutated. The *bis* mutant displayed patterning defects both in the anterior–posterior axis of the craniofacial skeleton and the dorsal–ventral axis of the caudal one. In the anterior region, the *bis* mutant exhibited craniofacial cartilage homeosis. The expression of *Hox* genes was decreased in the pharyngeal arches, suggesting that the pharyngeal segmental identities were altered in the *bis* mutant. In the posterior region, the *bis* mutant exhibited abnormal patterning of the caudal skeleton, which ectopically formed at the dorsal side of the caudal fin. The expression of *Zic* genes was decreased at the posterior region, suggesting that the dorsal–ventral axis formation of the posterior trunk was disrupted in the *bis* mutant. We also found that the MOZ-deficient mice exhibited an abnormal patterning of their craniofacial and cervical skeletons and a decrease of Hox transcripts. We propose a common role of the MOZ HAT complex in vertebrates, a complex which is required for the proper patterning for skeletal development.

Introduction

Determination of 3 axes, i.e., the anterior–posterior (A–P) axis, dorsal–ventral (D–V) axis, and left–right (L–R) axis, underlies the developmental processes of a vertebrate embryo as it forms from the fertilized egg to achieve the proper morphology (Beddington and Robertson, 1999; Kuratani, 2005). The A–P axis is governed by *Hox* genes, which encode homeodomain-containing transcription factors. *Hox* genes were first described in *Drosophila* for their ability to cause segmental homeotic transformation in the body plan (Lewis, 1978; Wellik, 2007). A co-linear relationship exists between the relative orders of *Hox* genes. Genes at the 3′ end of the Hox clusters are activated first in the most-anterior parts of the developing embryo, whereas genes located at the more 5′ genomic position of the Hox clusters are activated subsequently in the more posterior parts (Frohman et al., 1993; Kmita and Duboule, 2003; Kondo and Duboule, 1999). The existence of a 'Hox code' has been proposed to assign morphologies to each segment as a result of the combination of the expression of each *Hox* gene (Kuratani, 2005; Wellik, 2007).

Anteriorly, the craniofacial skeleton is derived from the head segmented pharyngeal arch, the fate of which is determined by *Hox* genes located at the 3′ end of the chromosome (Piotrowski and Nusslein-Volhard, 2000). For instance, targeted inactivation of Hoxa2 in mice causes homeotic transformation of the second arch to the skeletal element derived from the first arch with reverse polarity (Gendron-Maguire et al., 1993; Rancourt et al., 1995; Santagati et al., 2005). Posteriorly, the fate of the skeletal identity in the tail region is determined by *Hox* genes located at the 5′ end of the chromosome (Wellik and Capecchi, 2003). Targeted disruption of Hox13 groups results in an anterior shift of morphology of the vertebrae (Dolle et al., 1993; Economides et al., 2003; Godwin and Capecchi, 1998). Thus, the proper regulation of *Hox* genes is required for the proper morphology along the A–P axis.

The expression of *Hox* genes is regulated in dual phases: an early phase, in which the initial expression pattern of *Hox* genes is established along the A–P axis, and a late phase, in which the expression pattern is sustained during further development (Deschamps et al., 1999; Deschamps and van Nes, 2005). The initiation of the expression of *Hox* genes depends on fibroblast growth factor (Fgf) and retinoic acid (RA) signals, and the counter gradients of Fgf and RA signals control the A–P axis formation via regulation of the expression of these *Hox* genes (Bel-Vialar et al., 2002; Deschamps and

* Corresponding author. Fax: +81 45 924 5718.
E-mail address: akudo@bio.titech.ac.jp (A. Kudo).

0012-1606/$ – see front matter © 2009 Elsevier Inc. All rights reserved.
doi:10.1016/j.ydbio.2009.02.021

van Nes, 2005; Diez del Corral and Storey, 2004). Maintenance of stable expression patterns of the *Hox* genes is regulated by the *Polycomb*-group (PcG) and *Trithorax* group (TrxG) of proteins, which are involved in the epigenetic mechanism via modulating the chromatin structure. Previous reports have demonstrated that PcG proteins repress the expression of *Hox* genes, whereas TrxG proteins maintain the active state of their expression (Papp and Muller, 2006; Soshnikova and Duboule, 2008). In mammals, targeted disruption of PcG genes; *bmi*, *mel-18*, *m33*, and *rae28*, causes an anterior shift of the expression of *Hox* genes, which results in the homeotic transformation of vertebrae to posterior segmental identities (Akasaka et al., 1996; Akasaka et al., 2001; Core et al., 1997; del Mar Lorente et al., 2000; Suzuki et al., 2002; Takihara et al., 1997). Targeted disruption of a mammalian *trx* gene, *mll* in mice, causes a gradual reduction in the expression of *Hox* genes during development (Glaser et al., 2006; Yu et al., 1998, 1995). In addition, a histone acetyltransferase (HAT) of the MYST family, Moz (Myst3), which has been implicated to act as a TrxG, is required for the maintenance of the expression of *Hox* genes in the pharyngeal arches during zebrafish embryogenesis (Miller et al., 2004). Although these studies on PcG and TrxG genes have shown several alterations of *Hox* gene expression in restricted regions of developing embryos, PcG and TrxG functions in the transcriptional regulation of *Hox* genes, especially TrxG functions, have not been adequately demonstrated.

In this study, we isolated and characterized a mutant in medaka named *biaxial symmetries* (*bis*), a mutant which displays patterning defects not only in the A–P axis of its craniofacial skeleton but also in the D–V axis of its caudal fin. In the *bis* mutant, the craniofacial skeleton was homeotically transformed into one with anterior morphology. The expression of *Hox* genes was decreased in the pharyngeal arches in the *bis* mutant, suggesting that the segmental identities of pharyngeal arches had been disrupted. Positional cloning revealed a loss of Brpf1 function in the *bis* mutant. Brpf1, containing a bromodomain and PHD finger, is a TrxG member and a close partner of the MOZ HAT complex (Doyon et al., 2006; Rokudai et al., 2009). This study revealed that Brpf1 is essential for the maintenance of expression of *Hox* genes not only in the anterior region, but also in the posterior region. In the posterior trunk, disruption of Brpf1 function caused decreased expression of *Zic* genes, which regulate the D–V axis of the caudal fin. Furthermore, we characterized the skeletal abnormality of the MOZ-deficient mice, and demonstrated similar abnormalities between the *brpf1* medaka mutant and MOZ-deficient mice, thus implying a common role of the MOZ HAT complex in the skeletal patterning of vertebrates.

Methods

Medaka strains and mutant screening

The medaka (*Oryzias latipes*) strain Cab was used for all studies as the wild type. The *Da* mutant was purchased from local pet shops. The fish were maintained in an aquarium system with re-circulating water at 28.5 °C. Naturally spawned embryos were obtained, incubated at 28 °C, and staged as previously described (Iwamatsu, 2004). Eggs were maintained in the medaka Ringer's solution (0.65% NaCl, 0.04% KCl, 0.011% CaCl2, 0.01% $MgSO_4$, 0.01% $NaHCO_3$, 0.0001% methylene blue).

Mutagenesis using N-ethyl-N-nitrosourea (ENU) was performed according to a standard protocol established for zebrafish (Mullins et al., 1994; Solnica-Krezel et al., 1994; van Eeden et al., 1999), with some modifications (Tanaka et al., 2004). The male fish were exposed to 2.5 or 3 mM ENU for 2 h at room temperature in a buffer containing 0.03% instant ocean (Tetra) and 1 mM sodium phosphate buffer at pH 6.5. The ENU treatment was repeated at 7 days after the initial treatment. Three weeks after the second ENU treatment, these male fish were crossed with the wild-type females to produce families of F1 fish. The F1 fish were then mated to each other to obtain F2 families. For each F2 family, random crosses (up to 8 pairs) were made to obtain the F3 progeny. Embryos and larvae were observed for their mutant phenotypes under a stereomicroscope at 3 different stages (3, 5–6, and 9–10 days after fertilization).

Whole-mount RNA in situ hybridization and skeletal staining

Whole-mount RNA *in situ* hybridization using digoxigenin-labeled anti-sense RNA probes was performed as previously described (Inohaya et al., 1995, 1999). For cartilage staining with Alcian blue 8GX (Sigma), larvae were fixed with 4% paraformaldehyde (Sigma) in PBS at 4 °C overnight, washed twice in PBS containing 0.1% Tween (PBST) for 10 min, and stained with the Alcian blue solution (70% ethanol, 30% acetic acid containing 0.1% Alcian blue) at room temperature overnight. Larvae were hydrated by passage through a graded series of PBS and decolorized in a solution of 1% KOH and 0.9% hydrogen peroxide. Then the larvae were treated at room temperature for less than 1 h with 0.1% trypsin (DIFCO) in a 30% sodium borate saturated solution. The calcified bone was stained with Alizarin red S (Nacalai Tesque). For this staining, larvae were fixed in 4% paraformaldehyde with 0.05 N sodium hydroxide at 4 °C overnight. After a brief washing in PBST, the fixed larvae were stained by immersion in the Alizarin red solution (4% Alizarin red, 0.5% potassium hydroxide) at room temperature for several hours or overnight. Stained samples were stored in 80% glycerol and photographed. For visualization of the cartilage in whole mouse embryos (E14.5), embryos were fixed in 95% ethanol overnight and stained with Alcian blue solution (80% ethanol, 20% acetic acid containing 0.1% Alcian blue) for 24 h. They were then washed for 24 h in 95% ethanol. Cartilages were cleared with 1% KOH. Embryos were stored in 80% glycerol/1% KOH.

Positional cloning

The *bis* heterozygous fish maintained on the southern Cab genomic background were mated with the wild-type northern HNI fish to generate F1 families. Embryos for the genetic mapping were obtained from inter-crosses of the F1 *bis* carriers. For establishment of the initial genetic linkage, bulk segregant analysis was conducted on pools of genomic DNA from the *bis* mutants and wild-type embryos by using the sequence-tagged site (STS) markers on the medaka genome (Kimura et al., 2004). The genetic interval was narrowed down by the analysis of individual embryos by the use of additional STS markers, MF01SSA007H10 and MF01SSA044E03 (Naruse et al., 2000), and newly designed restriction fragment length polymorphism (RFLP) markers, CRELD and BICD2 [CRELD, 5′-AGATAGAAGAC-CAAGTGGAGACG-3′ and 5′-GTATCCTGGATCGCAGATGC-3′/HinfI; and BICD2, 5′-TCTGCGGACAGTCCTAAAGG-3′ and 5′-TTGGACAGAG-CAATCTCAGC-3′/HhaI]. cDNAs of *brpf1* from the *bis* mutants and the wild types were amplified in 2 groups of about 2000 base pairs (bps) and the sequences verified. To directly confirm the linkage between the *bis* locus and *brpf1*, we amplified a part of *brpf1* genomic DNA (primers 5′-GCTAAGGACACGGTGTTTTAC-3′ and 5′-GCTGCCTGGTAC-CATCTGTC-3′), and digested the PCR fragments with the restriction enzyme DdeI, which cleaves the mutant-type allele, but not the wild-type one. The nucleic acid sequence of medaka *brpf1* was deposited in the DDBJ/EMBL/GenBank. Accession No. AB488461.

Immunohistochemistry

Embryos were fixed with 4% paraformaldehyde/PBS for 2 h. After fixation, embryos were washed three times for 10 min each time with MABT (0.1% Triton-X-100 in MAB, which was 100 mM maleic acid and 150 mM NaCl, pH 7.5) and subsequently with MABDT (1% BSA and 1% DMSO in MABT) twice for 30 min each time. After having been blocked with 2% lamb serum in MABDT, embryos were incubated in the blocking solution containing the primary antibody (1:200; anti-Phospho-histone H3; Upstate) overnight at 4 °C. Embryos were

washed with MABDT three times for 5 min each time, four times for 30 min each time with 2% lamb serum in MABDT for blocking. Thereafter, embryos were incubated with the secondary antibody (1:1000; Alexa-488 conjugated anti-rabbit IgG; Molecular Probes) overnight at 4 °C. Then, embryos were washed with MABT and observed using a confocal microscope (Fluoview FV1000, Olympus).

Generation of construct and transgenic lines

A genomic fragment containing the *brpf1* promoter and Brpf1 coding sequence was amplified in 2 parts (5′ half and 3′ half fragments) from a BAC clone (ola148H10) by using the appropriate primers. The amplified fragments were cloned into the TA cloning vector. We then digested the 5′-half fragment with SalI and NotI, and subcloned it into the XhoI NotI sites of an I-SceI backbone vector, which contains two I-SceI sites (Thermes et al., 2002). The 3′-half fragment, digested with NcoI and NotI, was cloned into the NcoI site of the inserted 5′-half fragment and the NotI site of the vector. This plasmid was digested with I-SceI (New England Biolabs), and the fragments (20 ng/μl) were injected into the cytoplasm of 1-cell stage embryos. The embryos showing a transiently strong expression of the exogenous gene were allowed to grow to adulthood. We then checked the GFP expression in the next generation, and picked an embryo with stable integration of the injected construct as the transgenic line.

Determination of the genotype of the rescued *bis* mutant was performed by using ENU-induced polymorphism, which exists at the genomic region 70 kb separated from the *brpf1* mutation point. This polymorphism showed strong linkage with the *brpf1* mutation (0 recombinations per 980 meioses). It was difficult to use the *brpf1* mutation point itself for determining the genotype because of the rescue construct containing the wild-type *brpf1* sequence. The genomic fragment was amplified by using the following primers: forward, 5′-ACTTCTTCTGCTTCACATGTGAC-3′, and reverse, 5′-AGAGA-CAGTCCTGGTATTCGG-3′, and sequenced by means of direct sequencing for determination of the genotype.

Whole-mount in situ hybridization of mouse embryos

Whole-mount *in situ* hybridizations were carried out according to the established protocol (Kondo and Dubrule, 1999), using DIG-labeled riboprobes. Embryos were permeabilized with 10 μg/ml proteinase K for 15 min. Probes (*Hoxa3* (Manley et al., 2004), *Hoxa4* (Kawazoe et al., 2002), *Hoxd10* (Redline et al., 1992), *Hoxd11* (Izpisua-Belmonte et al., 1991)) were described previously.

Results

Isolation of a medaka mutant that exhibits pharyngeal cartilage homeosis

To investigate organogenesis of vertebrates, we performed a medium-scale screening of medaka mutants obtained by ENU

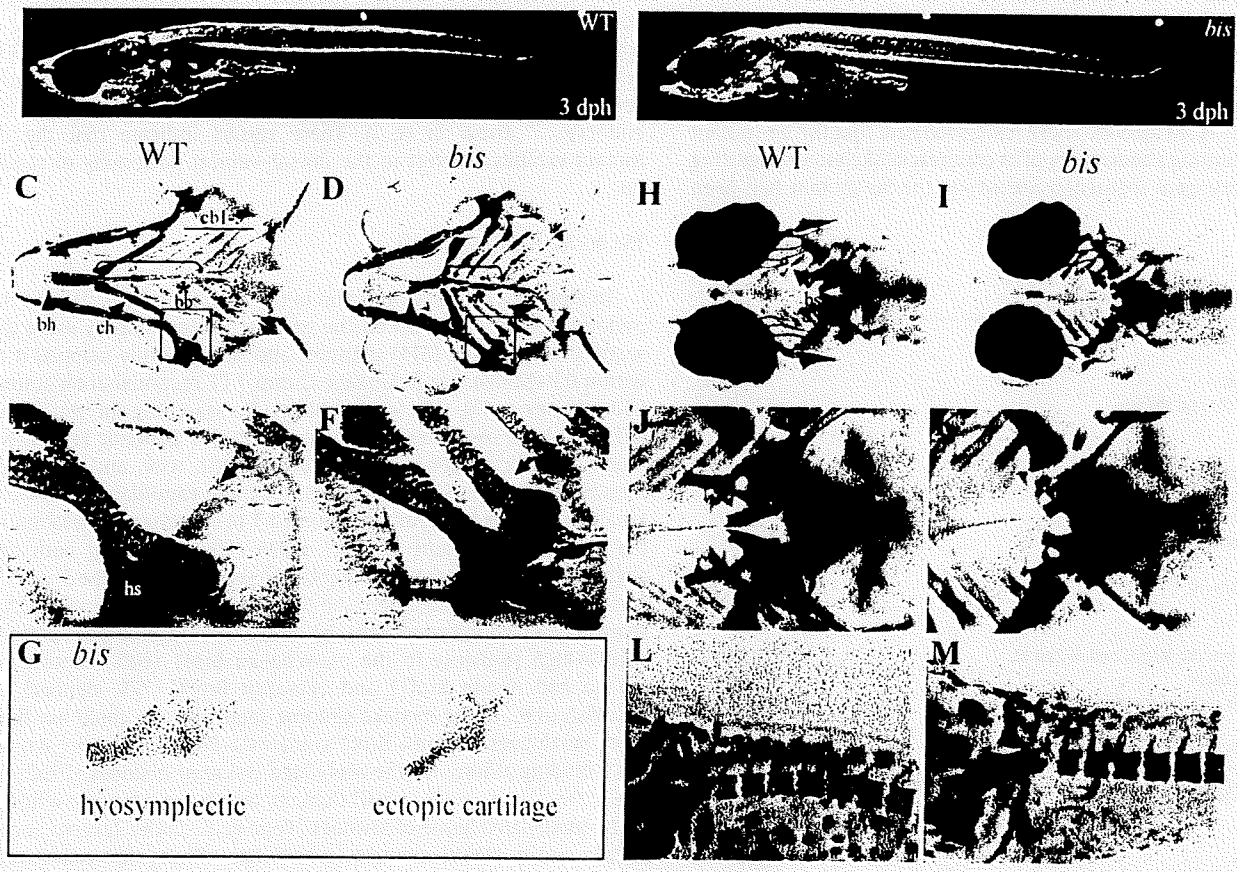

Fig. 1. The *bis* mutant displayed skeletal malformation. (A, B) Lateral view of a 3 dph larva. The *bis* mutant has a shrunken head. Other tissues appeared to have a normal morphology. (C–G) Craniofacial cartilage stained with Alcian blue. (C, D) Ventral view of wild-type and *bis* larvae. The bracket indicates the head region of the *bis* mutant and wild-type. Arrowheads indicate basihyal, which is decreased in the *bis* mutant; and arrows, the ceratohyal, which is short and thick in the mutant. (E, F) Highly magnified view of black boxed region in "C" and "D". The arrow in "F" indicates the ectopic cartilage at the lateral end of the first ceratobranchial in the *bis* mutant, compared with the wild-type (arrow in "E"). (G) View of a flat-mounted hyosymplectic and the ectopic cartilage of the *bis* mutant. The shape of ectopic cartilage has features characteristic of the hyosymplectic. (H–M) Calcified bone was stained with Alizarin red. (H, I) Ventral view of the wild type and the *bis* mutant. Arrows indicate the branchiostegal rays, which are decreased in number in the *bis* mutant. (J, K) Highly magnified view of the tooth region. Arrows indicate this region, where small pharyngeal teeth are seen in the *bis* mutant. (L, M) Lateral–dorsal view of the neck region. Arrows indicate the first vertebra, which is fused to the head in the *bis* mutant. bh, basihyal; ch, ceratohyal; cb 1–5, first to fifth ceratobranchial; bb, basibranchial; hs, hyosymplectic; bsr, branchiostegal ray; pt, pharyngeal tooth.

mutagenesis, and isolated the medaka mutant *biaxial symmetry* (*bis*). The *bis* mutant dies several days after hatching. Morphological examination showed the *bis* mutant to have a shrunken head (Figs. 1A, B). To visualize the craniofacial skeleton, we stained medaka larvae at 3 days post hatching (dph) with Alcian blue for cartilage. The craniofacial cartilage of the *bis* mutant was shrunk compared with that of the wild-type larvae (Figs. 1C, D). In the *bis* mutant, the length of each gill cartilage (ceratobranchials) was shorter, and the basihyal (derived from the second pharyngeal arch) was shortened compared with that of the wild-type larva (Figs. 1C, D, arrowhead and brackets). The ceratohyal (derived from the second pharyngeal arch) was shorter and thicker than that of the wild type (Figs. 1C, D, arrow). The second to the fifth ceratobranchials in the *bis* mutant were thicker and longer than those in the wild-type larvae (Figs. 1C, D). Although the basibranchial was separated in 2 parts in the wild-type larvae at the third ceratobranchial, the basibranchial was fused and extended to the fifth ceratobranchial in the *bis* mutant (Figs. 1C, D, asterisk). In addition, an ectopic cartilage was detected at the lateral end of the first ceratobranchial (derived from the third pharyngeal arch) on both sides of the head (Figs. 1C, D, square; E, F, arrow). An ectopic cartilage was often observed at the lateral end of the second ceratobranchial (Figs. 1C, D and Table 1). To further characterize the abnormalities of the *bis* mutant, we focused on the shape of the ectopic cartilage at the lateral end of the first ceratobranchial in the *bis* mutant. A flat-mounted observation revealed that the shape of the ectopic cartilage had the characteristic feature of the hyosymplectic, which is normally derived from the second pharyngeal arch (Fig. 1G). To observe the calcified bone, we stained the larvae with Alizarin red. Deformed brachiostegal rays (Figs. 1H, I arrow) and small pharyngeal teeth (Figs. 1J, K, arrow) were observed in the *bis* mutant. In the cervical region, the vertebra with neural arch was fused to the head skeleton in the *bis* mutant (Figs. 1L, M arrow). These results indicate that the *bis* mutant exhibits patterning abnormality of its craniofacial skeleton, suggesting that the pharyngeal segmental identity in the *bis* mutant had been disrupted.

Table 1
Skeletal phenotype of the *bis* mutant.

Cranio facial cartilage	n = 83
Arch2	
Basihyal reduced	83 (100%)
Ceratohyal shorter and thicker	83 (100%)
Arch3	
Ectopic cartilage at the lateral end of 1st cb	83 (100%)
Ectopic cartilage shape	
Small fragment	5 (6.0%)
Simple stick shape	16 (19.2%)
Similar to hs	62 (74.7%)
Hyobranchials absent	83 (100%)
Posterior arch	
Ectopic cartilage at the lateral end of 2nd cb	17 (20.4%)
Hyobranchials absent	83 (100%)
Ceratobranchials distally broadened	83 (100%)
Cervical and pharyngeal bone	n = 32
Fused vertebrate to head bone	28 (87%)
Reduced pharyngeal tooth	32 (100%)
Caudal skeleton	n = 50
Fused vertebrae	38 (76%)
Extra vertebra at the end of notochord	46 (90%)
Dorsally formed fin rays	50 (100%)
Reduced hypurals	43 (86%)

Percentage of animals with each phenotype was listed. Phenotypes of craniofacial cartilages were assessed by Alcian blue staining at 3 dph. Phenotypes of cervical and pharyngeal bone were assessed by Alizarin red staining at 3 dph and those of caudal skeletons were assessed by Alizarin red staining at 4 dph. These phenotypic differences of caudal skeleton were most likely caused by the subtle difference of the developmental stage in each animal.

The bis mutant exhibits defective skeletal patterning at the posterior region

The *bis* mutant exhibited disruption of the skeletal patterning not only in the anterior head region, but also in the posterior region. Compared with those of the wild-type larvae, the fin rays were ectopically formed at the dorsal region of caudal fin in the mutant (Figs. 2A, B, arrow); and the ossification pattern was disrupted at the caudal vertebrae in the *bis* mutant. An extra vertebra had formed at the end of the notochord in the *bis* mutant (Figs. 2A, B, arrowhead). In addition, the ossified hypural in the *bis* mutant was smaller than that of the wild type, and the hypural of the caudal most vertebra was deleted in the *bis* mutant (Figs. 2A, B, asterisk). Morphological analyses of embryos stained with Alcian blue revealed that the hypural was also ectopically formed at the dorsal side of the caudal fin and that each hypural was fused in the *bis* mutant (Figs. 2C, D, arrow). Furthermore, the blood vessels were ectopically extended at the dorsal side of the caudal fin in the *bis* mutant at 7 dpf (Fig. 2F, arrow) as opposed to their normal pattern in the wild type (Fig. 2E, arrow). To further characterize the caudal 287 fin abnormality of the bis mutant, we examined mitotic cells using mitotic marker phospho-histone H3 antibody at day 7 post fertilization (7 dpf), because the mesenchyme of the caudal fin, which exists at the ventral caudal end of the notochord, is known highly proliferative and involved in the development of the caudal fin (Hadzhiev et al., 2007; Sakaguchi et al., 2006). In the wild-type larvae, the mitotic cells largely existed at the ventral caudal end of the notochord (Fig. 2 arrow in G, I), as reported previously (Hadzhiev et al., 2007; Sakaguchi et al., 2006); whereas in the *bis* mutant, the mitotic cells existed not only at the ventral caudal end of the notochord but also at the dorsal caudal end (Fig. 2 arrow in H, I). These results indicate that the *bis* mutant exhibits a defect in the dorsal–ventral patterning of caudal fin.

The bis locus encodes brpf1

To identify a genomic mutation in the *bis* mutant, we mapped the mutated genomic position on the genetic linkage map by using the sequence-tagged site (STS) markers, and subsequently mapped it to within 0.1 cM distance in Linkage Group 7 (1 recombination among 980 meioses in Fig. 3A; see Methods). By searching for genes and ESTs that have been previously mapped to this genomic region, we found 3 predicted genes homologous to *fgd1*, *wnk*, and *brpf1*. We then sequenced the RT-PCR fragment of these candidate genes from *bis* and wild-type embryos, and found a T to A nonsense mutation in the open reading frame of *brpf1* cDNA (Fig. 3B). Using both the alignment of vertebrate Brpf1 amino acid sequences and the 5′ and 3′ race methods, we identified the medaka full-length *brpf1* cDNA sequence, which encoded 5451 bp and a 1283 amino acid protein with a high similarity to the mammalian Brpf1 (68% identical to human and mouse Brpf1) and zebrafish Brpf1 (77% identical to zebrafish one). In the medaka genome sequence, we could not find other paralogues of Brpf1. Brpf1 contains a BROMO domain, which has a binding affinity for the acetylated lysine of histones (Dhalluin et al., 1999; Yang, 2004); a PHD domain, which has a binding affinity for tri-methylated lysine of histones (Pena et al., 2006; Taverna et al., 2006); and a PWWP domain, which has affinity for condensed chromosomes (Laue et al., 2008; Turlure et al., 2006). In the *bis* mutant, the T to A transition introduced a stop codon (Y810Stop) at the end of BROMO domain, resulting in a truncated form of Brpf1 (Figs. 3B, C).

To examine the expression pattern of *brpf1*, we performed whole-mount RNA *in situ* hybridization on medaka embryos. The expression of *brpf1* was ubiquitous at st 21 (Fig. 3D), whereas at st 30 it was decreased in the trunk region and expressed in the

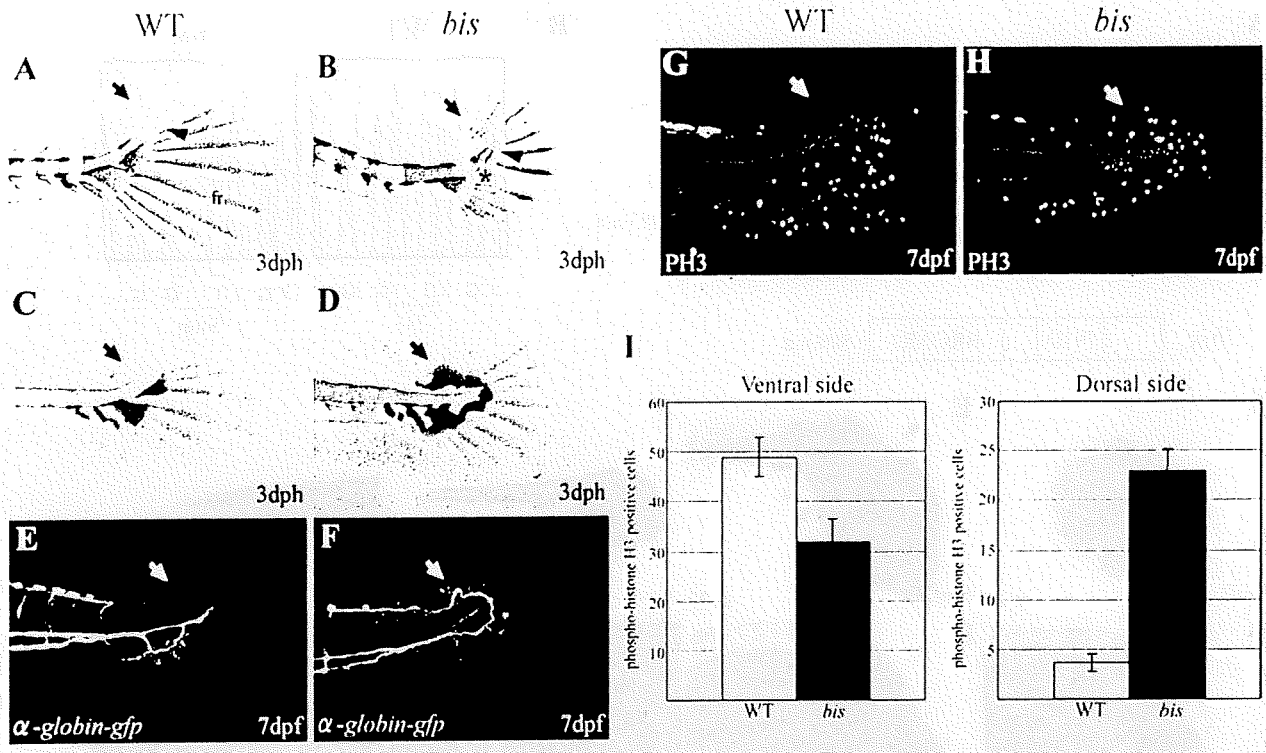

Fig. 2. The *bis* mutant exhibits D–V axis disruption in its caudal region. (A, B) Calcified bone of the caudal fin was stained with Alizarin red. A lateral view of the wild type and the *bis* mutant is shown. The arrow in "B" indicates the ectopic formation of fin rays at the dorsal region in the *bis* mutant; and that in "A" denotes its absence. The arrowhead in "B" indicates the abnormal patterning of the vertebra formed at the tip of the notochord, whereas that in "A" shows the normal patterning. In "B", the asterisk denotes the reduced or absence of hypurals in the *bis* mutant; and that in "A", the normal hypurals. (C, D) Cartilage of the caudal fin was stained with Alcian blue. A lateral view of the wild type and the *bis* mutant is shown. The arrow in "D" indicates the ectopic formation of the hypural cartilage at the dorsal side in the *bis* mutant, compared with the wild-type (arrow in "C"). (E, F) Blood vessels are visualized in the α-*globin*-GFP transgenic medaka. The blood vessel has ectopically extended at the dorsal side of the notochord in the mutant (F, arrow); and its absence there is indicated by the arrow in "E". (G, H) Mitotic cells were labeled with anti-phospho-histone H3 antibody. A lateral view of the caudal fin is shown. The arrow in "H" points to the ectopic proliferating cells at the dorsal side of the caudal region in the *bis* mutant, compared with the wild-type (arrow in "G"). (I) Histogram showing that mitotic cells were significantly increased at the dorsal side in the *bis* mutant. Error bar indicate S.D. fr, fin ray; hp, hypural.

pharyngeal arches and neural epithelium (Fig. 3E, arrow and arrowhead). The expression of *brpf1* was strong in the head region; however, the expression of *brpf1* was also detectable in the trunk and caudal region by long exposure at 4 dpf (Figs. 3F, G). In the *bis* mutant, *brpf1* mRNA could be detected, suggesting that the *bis* mutation does not affect the stability of *brpf1* mRNA and that the *bis* mutant produces truncated Brpf1 protein (Figs. 3H, I). In the *bis* mutant, the expression of *brpf1* mRNA existed, we then examined how this mutation affects the Brpf1 function by observing in vitro interaction with other members of the MOZ HAT complex and cellular localization of Brpf1. We generated the HA tagged human Brpf1 construct which contains the stop codon at the corresponding site to the *bis* mutation. By the *bis* mutation, the PWWP domain was deleted. Recently, it was demonstrated that the PWWP domain was not required for the interaction with Moz and Ing5 (Ullah et al., 2008). Consistent with this report, the truncated Brpf1 was normally interacted with Moz and Ing5 (Supplementary Figs. 1A–C). Although the truncated Brpf1 could be interacted with other members of the MOZ HAT complex, truncated Brpf1 was not co-localized with the condensed chromosome of mitotic cells (Supplementary Fig. 1D) as described previously (Laue et al., 2008; Turlure et al., 2006). These data suggest that the *bis* mutation causes the defect of Brpf1 function.

brpf1 is the gene responsible for the bis mutant

To confirm that the defects in the *bis* mutant were due to the genomic mutation in the *brpf1* gene, we rescued the *bis* mutant by introducing into the *bis* mutant the wild-type *brpf1* gene under the control of the genomic *brpf1* promoter region. To express the wild-type *brpf1* in an appropriate position and stage, we first obtained a genomic DNA fragment involving the 6-kb upstream region from the first methionine codon of the *brpf1* gene by the PCR. To check the ability of this promoter region to express the *brpf1* gene, we constructed an EGFP reporter vector and generated transgenic medaka. Fluorescent signals of EGFP were similar to the expression pattern of endogenous *brpf1* mRNA (Figs. 3J, K), suggesting the suitability of this 6-kb promoter region. We then generated a transgenic construct that contained the 6-kb promoter region, the genomic sequence encoding the *brpf1* gene, and the *crystalin* promoter-GFP that is used for checking the transgene integration into a chromosome (the construct is shown in Fig. 4A). We micro-injected the rescue DNA construct into the fertilized eggs of heterogenous mutants, picked up embryos with EGFP-positive eyes, and then inter-crossed the offspring to obtain the *bis* mutant harboring the rescue DNA construct. The *bis* mutant that had the rescue DNA construct developed normally, and was indistinguishable from the wild type. Histomorphometric analyses using Alcian blue and Alizarin red showed that the skeletal patterning of the rescued *bis* mutant indicated a restored normal morphology (Figs. 4B–J). These results confirm that the *brpf1* gene was responsible for the *bis* mutant.

Brpf1 is required for the maintenance of expression of Hox genes

The defect in the segment patterning along the A–P axis in the *bis* mutant implies that the faulty regulation of *Hox* gene expression by the chromatin structure (known as TrxG and PcG) is responsible for the *bis* mutant phenotypes, because Brpf1 is a component of the MOZ HAT complex (Doyon et al., 2006). To elucidate the involvement

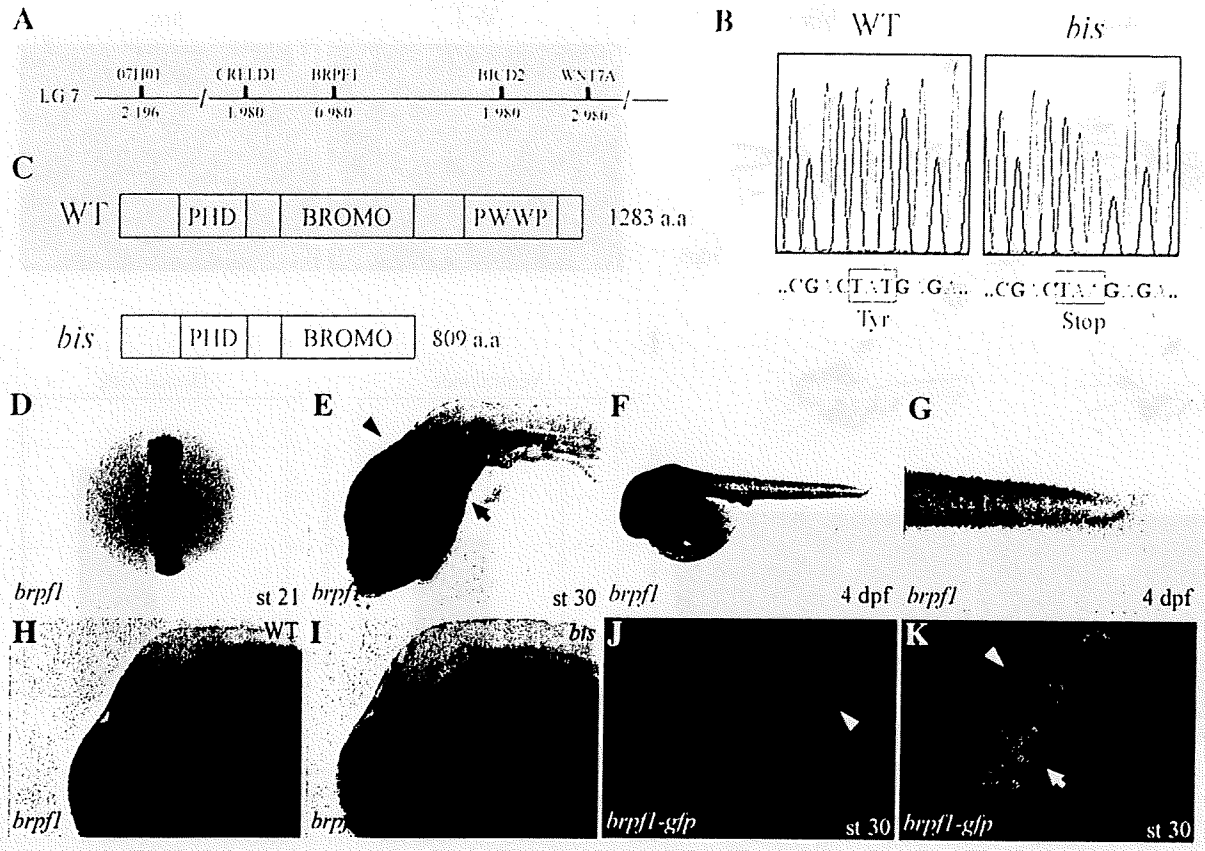

Fig. 3. The *bis* locus encodes the *brpf1*. (A) Genetic map of the *bis* locus in LG7. The number of recombinations is shown under the line. (B) The *bis* mutant has a T to A non-sense mutation in the *brpf1* gene. (C) Schematic of Brpf1 protein structure in the wild type and the *bis* mutant. The T to A transition results in the Y810Stop and thus generates a truncated Brpf1 protein with the bromo domain as its end in the *bis* mutant. (D–I) The expression pattern of *brpf1*. (D) *brpf1* is expressed ubiquitously at st 21. (E) The expression of *brpf1* became intense in the head at st 30. The arrow and arrowhead indicate the expression of *brpf1* at the pharyngeal arch and hindbrain, respectively. (F, G) The expression of *brpf1* at 4 dpf after long exposure. The expression of *brpf1* is observed in the trunk region and caudal end. (H, I) Lateral view of expression of *brpf1* in the wild type (H) and in the *bis* mutant (I) at st 30. The expression of *brpf1* is normal in the *bis* mutant. (J, K) Confocal microscope images of the *brpf1*-GFP transgenic medaka. The GFP signals are observed to have a pattern similar to that of the endogenous *brpf1* expression (J and K, arrowhead. Compare with the E and F). The intense signal was a non-specific signal due to pigment (arrow in "K").

of *Hox* genes in the *bis* phenotypes, we first examined the expression of *hoxa2a*, *hoxa3a*, *hoxa4a*, *hoxa5a*, *hoxb1a*, *hoxb2a*, *hoxb3a*, *hoxb4a*, and *hoxb5a* in medaka, which were previously reported to be expressed in the pharyngeal arches and involved in the establishment of the A–P axis identity of the pharyngeal arches and hindbrain in mice and zebrafish (Favier and Dolle, 1997; Kimmel et al., 2001). Although the expression of *hoxb1a* was maintained in rhombomere 4 during development of the wild-type at st 29 to st 31 (Supplementary Fig. 2A), the expression gradually decreased in the *bis* mutant (Supplementary Fig. 2B).

Hox2 and 3 group genes play a crucial role in determining the segmental identity at the second and third pharyngeal arches, respectively (Kimmel et al., 2001). We first examined the expression of Hox 3 group in the *bis* mutant, because the ectopic cartilage formation at the third pharyngeal arch implied the disruption of the segmental identity at the third arch in the *bis* mutant. The expression of both *hoxa3a* and *hoxb3a* was severely decreased at this pharyngeal arch and mildly decreased in the hindbrain of the *bis* mutant (Fig. 5A, B arrow and arrowhead in right panels), compared with that in the wild type (Figs. 5A, B arrow and arrowhead in left panels). Notably, the expression at the third pharyngeal arch was most affected and completely abolished in the *bis* mutant (Figs. 5A, B, line). These results suggest that the segmental identity of the third arch had transformed to become another segmental identity in the *bis* mutant. In other *Hox* genes, similar decrease was observed in the *bis* mutant (Supplementary result and Supplementary Figs. 2C, D).

These *Hox* genes were normally expressed in the early stage (st 22–27) in the *bis* mutant (data not shown). These results suggest that Brpf1 is involved in the maintenance of the expression of *Hox* genes in the pharyngeal arches.

The segmental identities are disrupted in the pharyngeal arch in the bis mutant

The maintenance of the expression of *Hox* genes is essential for the establishment of the segmental identity of the pharyngeal arches (Santagati et al., 2005). The segmental identities of pharyngeal arches are defined by the expression of *goosecoid* (*gsc*) and *bapx1*, which are essential for the proper patterning of the craniofacial cartilage (Rivera-Perez et al., 1995; Tucker et al., 2004). To investigate the effects of decreased expression of *Hox* genes on pharyngeal arch identities in the *bis* mutant, we examined the expression of *gsc* and *bapx1* at the late stage (st 30), when the expression of *Hox* genes was severely decreased in the pharyngeal arches in the *bis* mutant. Although *gsc* was expressed in the first and second pharyngeal arches in the wild type, an ectopic expression of *gsc* was detected in the third and fourth arches in the *bis* mutant (Fig. 5C, arrows in upper panels). The expression of *gsc* in the fifth to seventh pharyngeal arches corresponding to the putative pharyngeal teeth was decreased in the *bis* mutant (Fig. 5C, arrowheads in lower panels), arches which correspond to the putative pharyngeal teeth. The expression of *bapx1* at the pharyngeal arch was also anteriorized in the *bis* mutant (Supplementary result and Supplementary Figs. 3A, B). In mice,

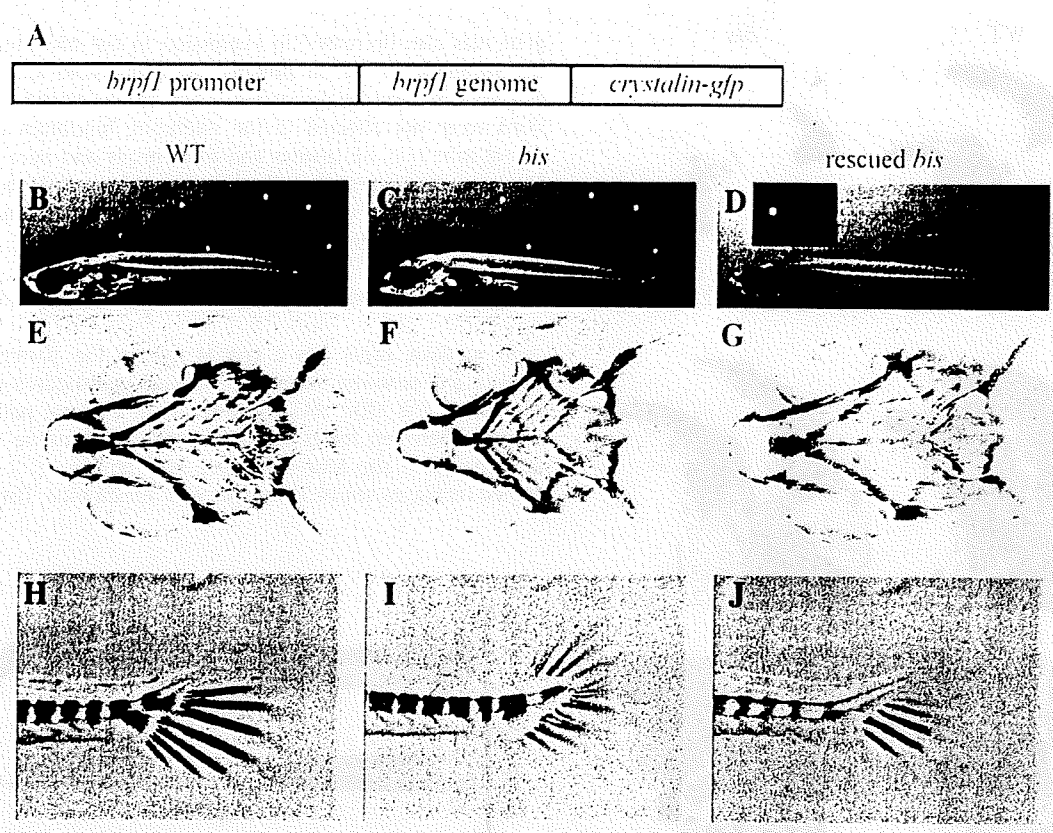

Fig. 4. *brpf1* is responsible gene for the *bis* mutant (A) Schematic of the rescue DNA construct. This construct contains the 6-k *brpf1* promoter, genomic sequence coding for the Brpf1 protein, and *crystalin* promoter-GFP. (B–D) The lateral view of the wild-type (B), *bis* (C), and rescued *bis* larva (D) at 3 dph is shown. Rescue construct-treated *bis* mutants show restoration of the normal morphology. The inset in "D" shows the expression of GFP in lens. (E–G) Ventral view of craniofacial cartilage of the wild type (E), *bis* (F), and rescued *bis* larva (G) stained with Alcian blue. The ectopic cartilage and shrunken gill arches were not observed in the rescued *bis* mutant. (H–J) The lateral view of caudal fin rays of the wild-type (H), *bis* (I), and rescued *bis* (J) larvae stained with Alizarin red. Ectopically formed dorsal fin rays are not observed in the rescued *bis* mutant.

inactivation of *hoxa3* gene results in the defect in thymus formation (Le Douarin and Jotereau, 1975; Manley and Capecchi, 1997, 1998). Then, we investigated *rag1* expression which was expressed in the hematopoietic cells at the thymus (Willett et al., 1997). In the *bis* mutant, *rag1* expression was reduced compared with the wild type (Supplementary result and Supplementary Fig. 3C). These results indicate that the segmental identity of pharyngeal arches was altered to the anterior identity in the *bis* mutant.

Brpf1 is required for the maintenance of Hox gene expression in the posterior region

The decreased expression of *Hox* genes in the anterior region can account for the anterior transformation of the pharyngeal arch in the *bis* mutant, whereas it still remained unclear how this decreased expression would result in the defect in the caudal fin. To clarify the caudal fin phenotype of the *bis* mutant, we focused on the Brpf1 function that is required for the maintenance of the expression of the posterior *Hox* genes. We then investigated the expression of *Hox* genes that are expressed in the caudal trunk region (*hoxa13a*, *hoxc11a*, *hoxc12a*, *hoxc13a*, *hoxd11a* and *hoxd12a*). Although *hoxc11a* was expressed in the caudal trunk in the wild type at 4 to 6 dpf, its expression gradually decreased in the *bis* mutant at 4 to 6 dpf (Fig. 6A). Expression of *hoxc12a* was detected in the caudal trunk region in the wild type. In the *bis* mutant, this expression was decreased at 4 to 6 dpf (Fig. 6B). The *hoxc13a* gene was expressed in the tip of the wild-type tail; whereas, in the *bis* mutant, the expression gradually decreased at 4 to 6 dpf (Fig. 6C). For other *Hox* genes, a similar decrease was observed in the *bis* mutant (Supplementary Figs. 4A–C). Then, to investigate whether Brpf1 has a role in the maintenance of the expression of all *Hox* genes, we examined the expression of *Hox* genes located at the center of the Hox cluster. In the *bis* mutant, the expression of *hoxa9a*, *hoxb6a*, and *hoxb8a* were not affected, and the expression of *hoxb9a* was mildly decreased. On the other hand, the expression of *hoxd10a* was severely decreased in the *bis* mutant (Supplementary Figs. 5A–E). These results suggest that Brpf1 is required for the maintenance of the expression of the anterior and posterior *Hox* genes but not for that of the center *Hox* genes.

The caudal skeletal phenotypes of the bis mutant were similar to those of the double anal n mutant (Da) in medaka

Posteriorly, the *bis* mutant exhibited the abnormality of D–V axis formation at the caudal fin. Then, we focus on the *Da* mutant which exhibits abnormal D–V axis formation in its somite and epithelial derivatives (Ohtsuka et al., 2004). To elucidate the similarity and difference between phenotypes of the *bis* mutant and those of the *Da* mutant in the caudal tissue, we compared the caudal skeletal abnormalities between the 2 mutants. The phenotype of caudal fin in the *bis* mutant was very similar to that of the *Da* mutant (Figs. 7A, B, arrows; C, D, arrows), implying that a similar mechanism was disrupted in the caudal fin of the *Da* and *bis* mutant. On the other hand, the extra vertebra and fused hypurals were not observed in the *Da* mutant (Figs. 7A, B, arrowheads; C, D). We then elucidated whether the expression of *Hox* genes was affected in the posterior region in the *Da* mutant. Although the expression of *hoxa13a* and *hoxc13a* in the posterior region was severely decreased in the *bis* mutant (Supplementary Fig. 4A and 6C), the expression of these *Hox* genes was normally expressed in the *Da* mutant (Figs. 7E, F). This result suggests that the expression of *Hox* genes is not directly linked with the appropriate D–V axis formation of the caudal fin.

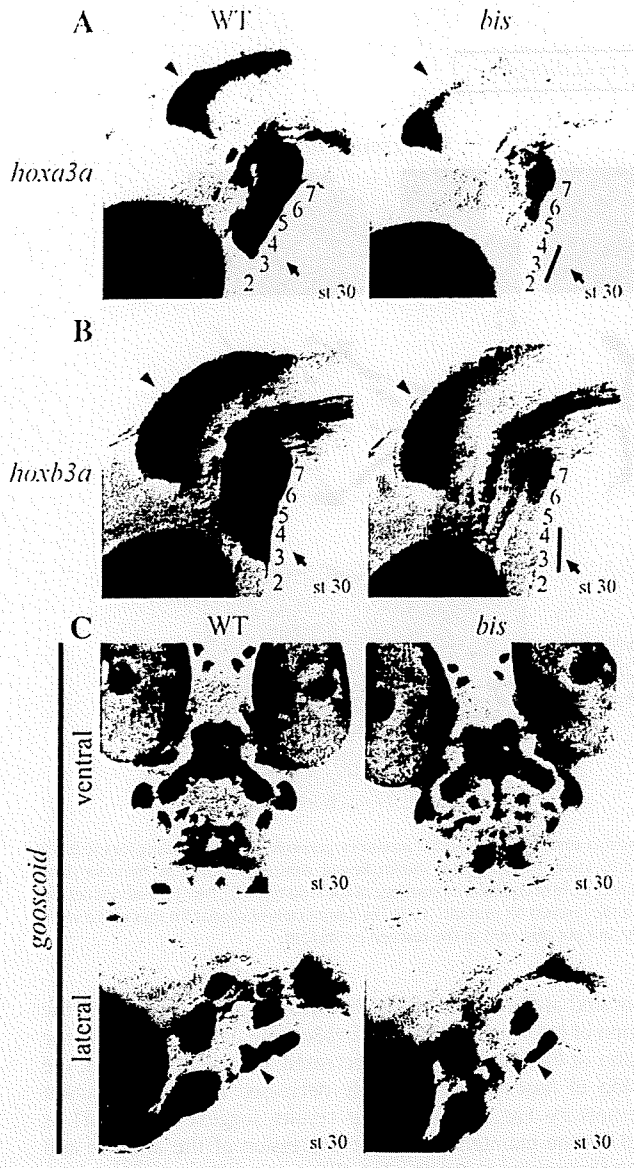

Fig. 5. Brpf1 is essential for the maintenance of expression of *Hox* genes and establishment of identities of pharyngeal arch. Developmental stages are indicated in lower right corners. (A) Expression of *hoxa3a* in the wild type and the *bis* mutant. Arrows indicate the expression, which is decreased in the third and fourth pharyngeal arches. (B) Expression of *hoxb3a* in the wild-type and the *bis* mutant. Arrows indicate the expression, which is reduced in the third and fourth pharyngeal arches. Note that the decrease in the levels of expression of *Hox* genes in the hindbrain was less severe than in those of *Hox* genes in the pharyngeal arches (arrowhead and arrow, respectively, in "A, B"). (C) Upper panels show ventral views and lower panels show lateral views of expression of *goosecoid* (*gsc*) in the wild type and the *bis* mutant. Arrows indicate the expression, which is ectopic in the third and fourth pharyngeal arches in the *bis* mutant. Arrowheads indicate the expression in the fifth to seventh pharyngeal arches, which is decreased in the *bis* mutant.

Expression of Zic genes is decreased in the posterior trunk region of the bis mutant

The *Da* mutant has 2 insertions near the *zic1* and *zic4* genes, resulting in the decreased expression of *zic1* and *zic4* genes at the dorsal somite in the *Da* mutant (Ohtsuka et al., 2004). To investigate the D–V axis formation governed by *Zic* genes in the *bis* mutant, we examined the expression of *zic1* and *zic4* genes in it. The expression of the *zic1* gene gradually decreased in the dorsal neural tube and somatic cells in the *bis* mutant from 4 to 6 dpf, compared with that in the wild type (Figs. 8A, B). The *zic4* gene was also decreased in expression in the *bis* mutant (Fig. 8C, D). Although, in the *bis* mutant, the expressions of *zic1* and *zic4* genes were severely decreased at the caudal tissue, their expressions were not affected in the midbrain, hindbrain and anterior neural tube (Fig. 8E, arrows and arrowheads and data not shown). These results suggest that the disruption of the D–V axis formation at the caudal fin in the *bis* mutant was due to the decreased expression of *Zic* genes in the posterior trunk.

MOZ HAT complex has a common role in the skeletal patterning

In medaka, Brpf1 has a crucial role in the patterning of the anterior and posterior skeletons. We then investigated whether the function of the MOZ HAT complex in the skeletal patterning was common between fishes and mammals. To examine the skeletal abnormality in the Moz−/− mice (Katsumoto et al., 2006), we stained cartilages of E14.5 embryos with Alcian blue. The lesser horn

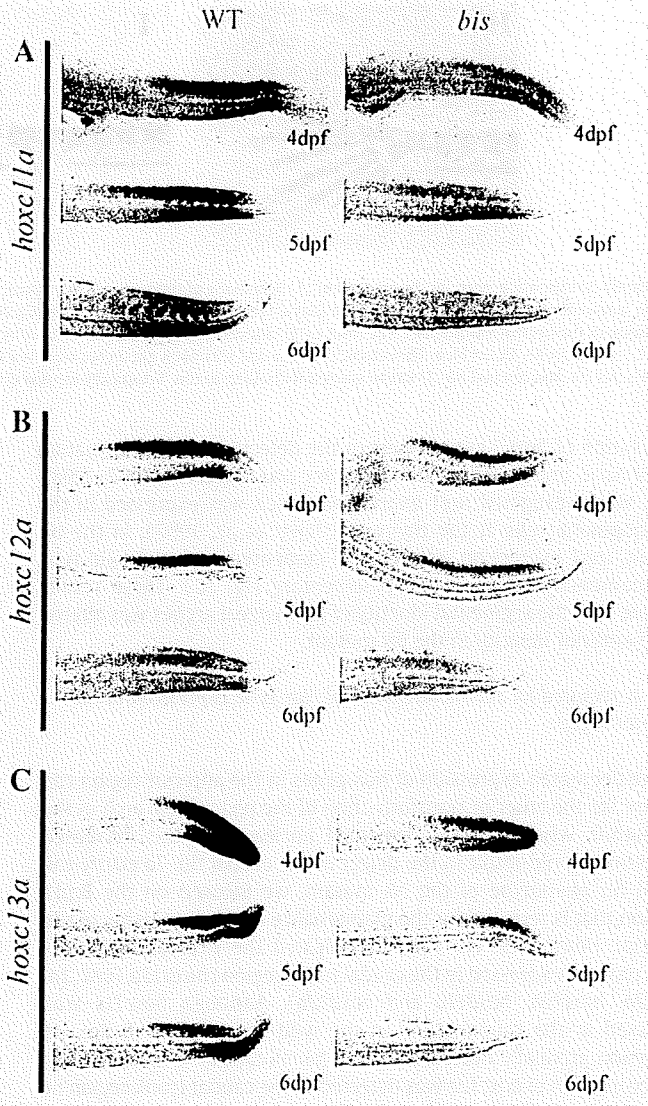

Fig. 6. Brpf1 is required for the regulation of expression of posterior *Hox* genes. Developmental stages of the embryo are indicated in the lower right corners, and lateral views are shown for all photos. (A) Expression of *hoxc11a* in the wild type and the *bis* mutant. The expression of *hoxc11a* gradually decreases in the *bis* mutant. (B) Expression of *hoxc12a* in the wild type and the *bis* mutant. The expression of *hoxc12a* is also decreased in the *bis* mutant. (C) Expression of *hoxc13a* in the wild type and the *bis* mutant. The expression of *hoxc13a* has completely decreased by 6 dpf in the *bis* mutant.

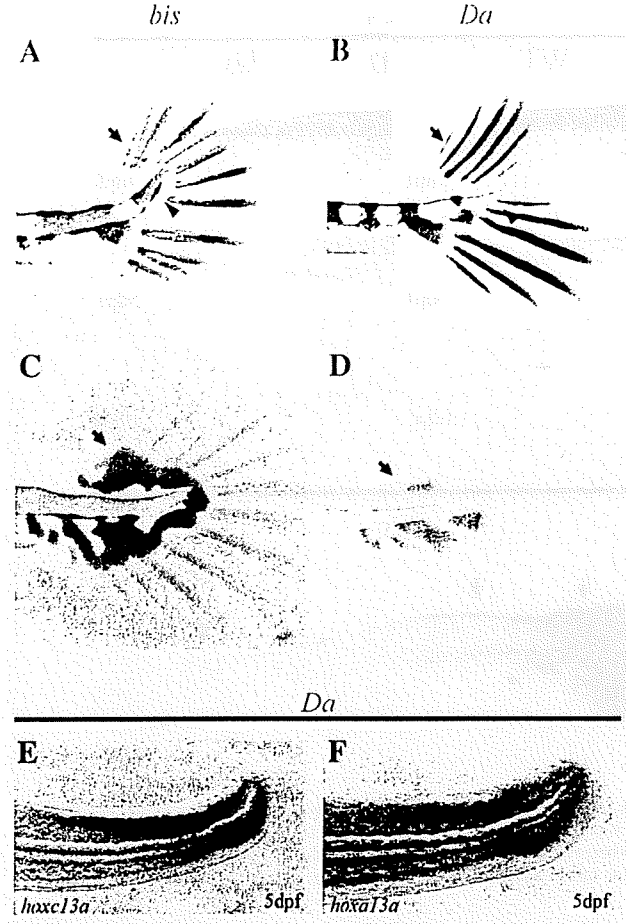

Fig. 7. The *Da* mutant exhibits a caudal fin phenotype similar to that of the *bis* mutant. Lateral views are given for all photos. (A, B) Caudal skeleton stained with Alizarin red at 3 dph. Ectopic dorsal formation of fin rays is evident in both the *bis* mutant and the *Da* mutant (arrow). However, evidence of ectopic formation of vertebrae is not observed in the *Da* mutant (arrowhead), though it is in the *bis* one (arrowhead). (C, D) Cartilage stained with Alcian blue at 3 dph. Evidence of ectopic dorsal formation of hypurals is seen in both the *bis* mutant (arrow) and the *Da* mutant (arrow). However, the fused hypurals are not observed in the *Da* mutant. (E) Expression of *hoxc13a* in the *Da* mutant. (F) Expression of *hoxa13a* in the *Da* mutant. The expression of *hoxc13a* and *hoxa13a* is normal in the *Da* mutant.

of the hyoid is derived from the second pharyngeal arch; and the greater horn, from the third pharyngeal arch. Moreover, the hyoid body is derived from the second and third pharyngeal arches (Lumsden et al., 1991; Noden, 1978, 1988). In the ventral view of hyoid cartilage, the shape of the hyoid body was changed rostrally to an acute shape in the Moz−/− mice (Figs. 9A–G); and in the anterior view, the lesser horn of hyoid was seen to have fused to the hyoid body in the Moz−/− mice (Figs. 9C, D, G). In the dorsal-lateral view, an accessory projection was observed on the greater horn of the hyoid in the Moz−/− mice (Figs. 9E, F, G). Although in the Moz−/− mice, a small ectopic cartilage was formed adjacent to the styloid process, other structures derived from the second pharyngeal arch were not affected in the Moz−/− mice (Supplementary Figs. 7A–D). In the *bis* mutant, the first cervical vertebra was fused to the head skeleton. So we examined the cervical skeleton of the Moz−/− mice. The neural arches of the cervical vertebrae were fused, and those of the axis and C3 were thickened in Moz−/− mice (Figs. 9H, I). Notably, the morphological feature of C3 neural arch has changed to that of axis (Figs. 9H, I, asterisks). In addition, the atlas was fused to the exoccipitals in the Moz−/− mice (Figs. 9J–M). In the posterior region, the Moz−/− mice had a kinky tail, although we failed to find an abnormality of posterior cartilage formation in the Moz−/− mice (Supplementary Figs. 7E, F). These results suggest that the MOZ HAT complex plays an essential role for the proper skeletal patterning in mice.

MOZ HAT complex was required for the transcriptional regulation of anterior and posterior Hox genes in mice

Moz−/− mice exhibited the similar phenotype in cervical cartilage to that in Hox4 deficient mice (Horan et al., 1995). We then examined whether the MOZ HAT complex was required for the maintenance of expression of *Hox* genes. The expression of *Hoxa3* and *Hoxa4* were mildly decreased at the rhombomere and neural tube in Moz−/− mice (Figs. 10A, B, arrowheads). On the other hand, their expressions were severely reduced at the somite (Figs. 10A, B, arrows). Consistent with the observation of the medaka *brpf1* mutant, in Moz−/− mice, the expressions of *Hoxa3* and *Hoxa4* were also decreased at the third and fourth pharyngeal arch, respectively (Figs. 10A, B, arrows in lower panels). Although the decrease of *Hoxa3* expression was observed, it was less severe than that of *Hoxa4* expression at the pharyngeal arch. Furthermore, we examined the expression of posterior *Hox* genes; *Hoxd10* and *Hoxd11*. In Moz−/− mice, the expressions of *Hoxd10* and *Hoxd11* were also reduced at the somite (Figs. 10C, D, arrows). These results suggest that, in mice, the MOZ HAT complex were also required for the maintenance of the expression of anterior and posterior *Hox* genes.

Discussion

In this study, we characterized the *bis* mutant in medaka, which exhibits defects in the development of its craniofacial and caudal skeletons. The expression of *Hox* genes was decreased during development of the *bis* mutant, compared with that of the wild type. Genetic analysis and the rescue experiment demonstrated that the loss of Brpf1 function was the cause of the *bis* phenotypes. Brpf1 is a partner of the MOZ HAT complex, which is essential for the maintenance of the expression of *Hox* genes, suggesting that the segmental identities along the A-P axis, which are governed by *Hox* genes, are disrupted in the *bis* mutant. Thus, we conclude that Brpf1 maintains the expression of *Hox* genes by regulating the modification of chromatin.

Brpf1 behaves as a part of the MOZ HAT complex functionally in skeletal development

Brpf1 contains multiple domains with the affinity for the modulated histone tail, suggesting that Brpf1 regulates transcription via modulating the chromatin structure. Previous studies showed that Brpf1 is a member of the MOZ HAT complex (Doyon et al., 2006; Yang and Ullah, 2007). Targeted inactivation of Moz in mice resulted in reduced hematopoiesis and decreased expression of *Hoxa9* gene in fetal liver (Katsumoto et al., 2006; Thomas et al., 2006). In addition, spleen formation was disrupted in the Moz−/− mice. We also observed that spleen formation was disrupted in the *bis* mutant (data not shown). ENU-induced mutation of the *moz* gene in zebrafish causes the homeotic transformation of the craniofacial cartilage and the decreased expression of *Hox* genes in the pharyngeal arches (Crump et al., 2006; Miller et al., 2004). Recently, phenotypes of the ENU-induced zebrafish mutant *brpf1* were shown to be similar to those of the zebrafish *moz* mutant, and the expression of *Hox* genes in the pharyngeal arches was decreased in the zebrafish *brpf1* mutant (Laue et al., 2008). Consistent with these previous reports, the *bis* mutant exhibited the anterior transformation of craniofacial cartilage and the deceased expression of *Hox* genes. In this study, we performed the *brpf1* morpholino anti-sense oligo experiment; however we failed in the phenocopy of *bis* mutant (data not shown), because the developmental stage of the establishment of pharyngeal arch

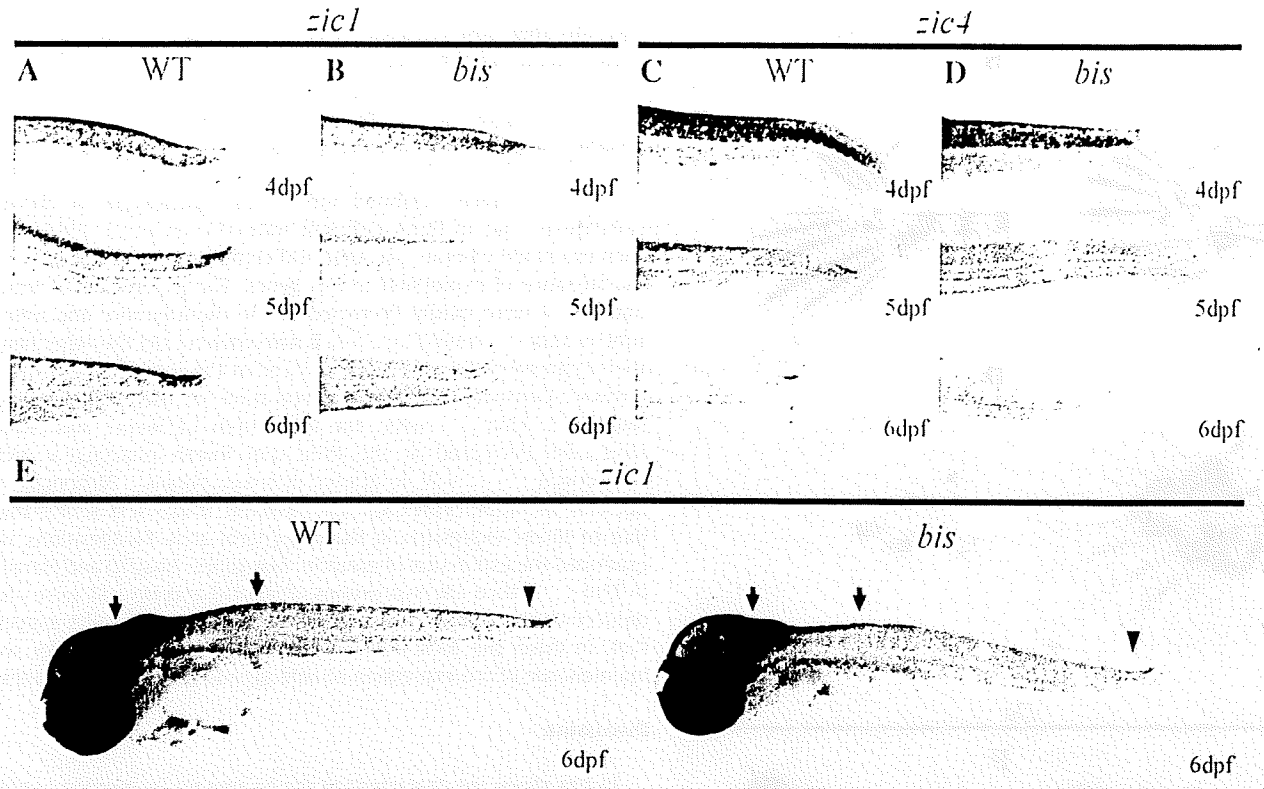

Fig. 8. The *bis* mutant exhibits decreased expression of *Zic* genes. Lateral views are given in all photos. (A, B) Expression of *zic1* in the posterior region in the wild type and the *bis* mutant. Although the expression of *zic1* is normally expressed in the *bis* mutant at 4 dpf, the expression gradually decreases at 5 and 6 dpf. (C, D) Expression of *zic4* in the posterior region in the wild type and the *bis* mutant. The expression of *zic4* is normal in the *bis* mutant at 4 dpf, whereas it gradually decreases at 5 and 6 dpf. (E) Lateral view of the expression of *zic1* in the wild type and *bis* larvae. Although the expression of *zic1*was decreased at the caudal tissue (arrowhead), it was not affected in the anterior neural tube and hindbrain (arrow).

identity in medaka was later than that in zebrafish. Alternatively, we demonstrated that re-introduction of the normal *brpf1* gene into the *bis* mutant could rescue the *bis* phenotype, and inhibition of HDAC activity partially rescued the phenotype of *bis* mutant (Supplementary result, Supplementary Fig. 6 and Supplementary Table 1); although, the efficiency of TSA treatment in the *bis* mutant was significantly lower than that of the zebrafish *moz* and *brpf1* mutants, probably due to the different sensitivity to TSA between two species. Thus, we suggest that Brpf1 behaves as a part of MOZ complex functionally in skeletal development.

The decreased expression of Hox genes in the pharyngeal arches causes homeotic transformation in the bis mutant

Our study demonstrates that Brpf1 is required for the proper patterning of the craniofacial cartilage, which is derived from neural crest cells that migrate from the hindbrain. Hox signaling has been implicated in the establishment of segmental identities of cranial neural crest cells. Hox2-group genes determine the identity of the second arch. A mutation in the *Hoxa2* gene in mice or knock down of *hoxa2b* and *hoxb2a* genes in zebrafish leads to a homeotic transformation of the second arch to the first arch identity (Gendron-Maguire et al., 1993; Hunter and Prince, 2002). The *bis* mutant exhibited the partial transformation of the second arch to the first identity, which is consistent with the deceased expression of the *hoxb2a* gene. Although zebrafish *moz* and *brpf1* mutants exhibited a complete transformation of the second arch identity to the first arch identity, the skeletal transformation of the second arch element was not significant in the *bis* mutant. This phenotypic difference between zebrafish and medaka may be due to the difference in the Hox cluster evolution. For example, although the expression of *hoxa2a* was maintained in the second pharyngeal arch in the *bis* mutant, *hoxa2a* does not exist in zebrafish (Hoegg et al., 2007; Kurosawa et al., 2006), suggesting that a Hox paralogue group, *hoxa2a*, has a functional redundancy in determining the A–P axis identity in the *bis* mutant. Thus, in the disruption of Brpf1 function, the other redundant mechanism may act in the maintenance of the expression of *hoxa2a*.

The *bis* mutant displayed decreased expression of *Hox3* genes and ectopic expression of *gsc* in the third pharyngeal arch, implying that the segmental identity of the third pharyngeal arch had changed to that of the second pharyngeal arch in the *bis* mutant. A loss of the thymus in the Hox3 group knock-out mice is consistent with that in the *bis* mutant (Manley and Capecchi, 1995, 1998). Furthermore, the fusion of the first vertebra to the head skeleton in the *bis* mutant probably corresponds to the similar phenotype in the Hox3 group knock-out mice (Condie and Capecchi, 1994; Manley and Capecchi, 1997). Although skeletal phenotypes of knock-out mice of the Hox3 paralogue group did not display an apparent transformation of the third arch-derived structure, the decreased expression of *Hox3* genes in the *valentino* mutant of zebrafish and the *kreisler* mutant of mice causes ectopic cartilage formation in the third pharyngeal arch, whose characteristic features resemble the hyoid derived from the second arch (Frohman et al., 1993; Manzanares et al., 1999; Moens et al., 1998; Prince et al., 1998). Thus, the decreased expression of *Hox3* genes might cause the homeotic transformation of the third arch identity into the second arch identity in the *bis* mutant.

The abnormality in D–V axis formation in the caudal n occurs due to decreased expression of Zic genes in the bis mutant

The *bis* mutant exhibited abnormalities in its posterior skeletal patterning. Although these phenotypes were not described in *moz*

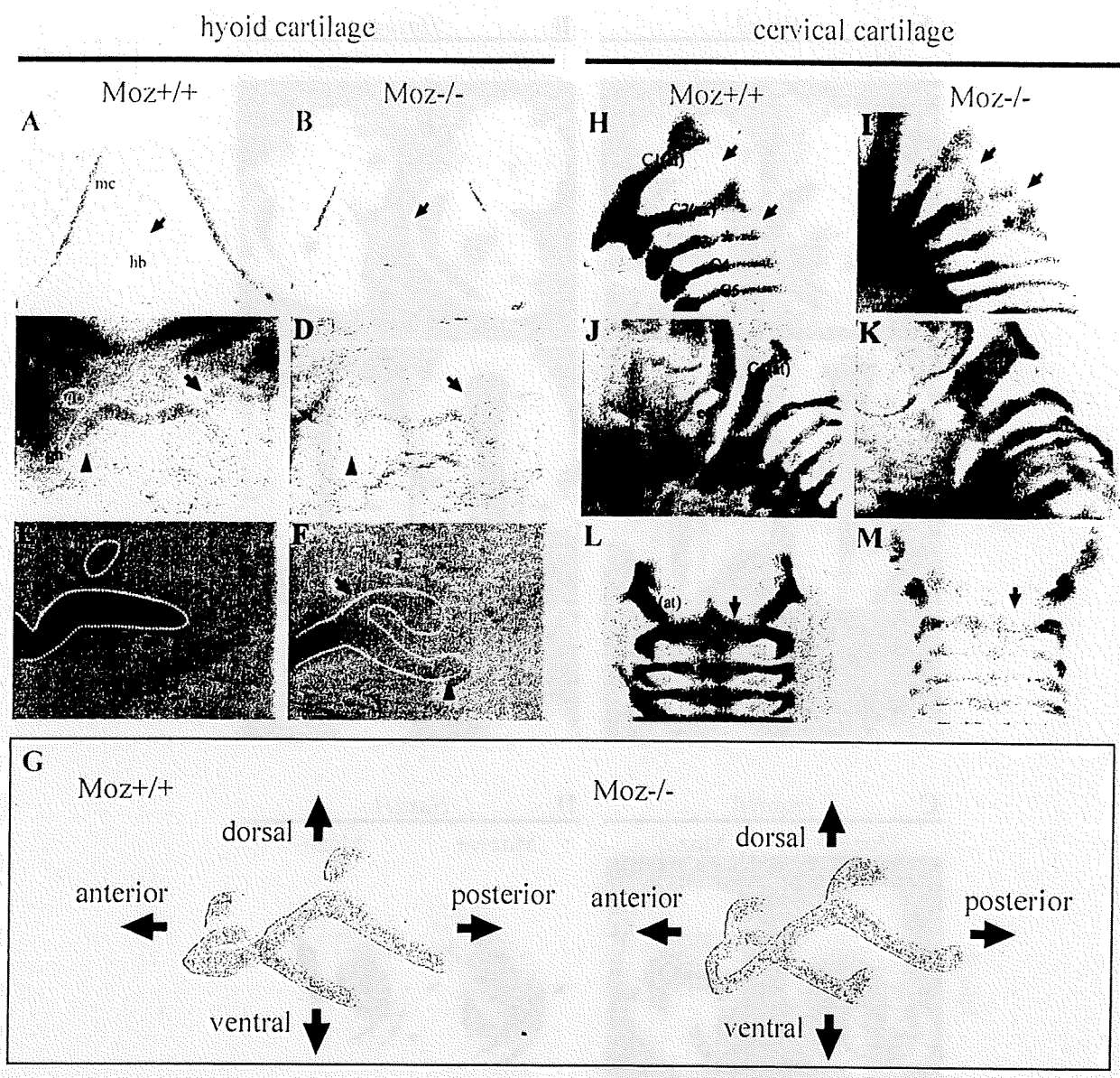

Fig. 9. Moz−/− mice exhibit abnormal patterning in hyoid and cervical cartilages (A–F). The hyoid cartilage was stained with Alcian blue. (A, B) Ventral views of the hyoid cartilage. The hyoid body is seen (arrows), which in the Moz−/− mice has morphological similarity to Meckel's cartilage. (C, D) Anterior views of the hyoid cartilage. The lesser horn of the hyoid (arrows) has fused to the hyoid body in the Moz−/− mice but not in the wild type; and an accessory process is notable on the greater horn of the hyoid in the mutant (arrowhead) but is absent in the wild-type (arrow indicating its absence). (E, F) Dorsal–lateral view of the greater horn of the hyoid, showing the same phenotypes as seen in the anterior view. (G) A schematic of the hyoid cartilage in the wild type +/+ and Moz−/− mice. (H–M) Cervical cartilages were stained with Alcian blue. (H, I) Lateral views of the cervical cartilage. The neural arches of atlas, axis, and C3 (arrows) are fused in the Moz−/− mice. The morphological feature of the neural arch of C3 (asterisks) has changed to that of the axis. (J, K) Dorsal–lateral views of the cervical cartilage. The atlas (arrows) has fused to the exoccipital in the Moz−/− mice. (L, M) Dorsal views of the cervical cartilage. The ventral part of the atlas (arrows) has been deleted in the Moz−/− mice. mc, Meckel's cartilage; hb, hyoid body; lh, lesser horn of hyoid; gh, greater horn of hyoid; C1–C5, cervical vertebra 1 to 5; at, atlas; ax, axis.

and *brpf1* mutants in zebrafish, the expression of *brpf1* itself exists in the posterior trunk region in zebrafish (ZFIN: MGC55530). The *bis* mutant exhibited the D–V axis disruption in its caudal fin. Our study revealed that the expression of *zic1* and *zic4* genes in the posterior trunk region was severely decreased in the *bis* mutant, suggesting that the disruption of the D–V axis was due to the decreased expression of these genes.

The *bis* mutant also exhibited decreased expression of *Hox* genes in the posterior trunk region. It should be noted that their expression decreased earlier than that of *Zic* genes in the posterior region (Figs. 6 and 8). Furthermore, in the *Da* mutant, *Hox* genes were normally expressed in the posterior region. Although no other previous reports have described the relationship between *Hox* genes and *Zic* genes *in vivo*, the Chip-on-Chip assay for Hoxa13 showed that the Hoxa13 protein binds to the *zic1* and *zic4* promoter sequence (Rinn et al., 2008). Therefore, our findings suggest that Brpf1 regulates the expression of *Zic* genes via the regulation of *Hox* genes.

The decreased expression of Hox genes causes the abnormal patterning of caudal vertebrae in the bis mutant

The *bis* mutant exhibited similar phenotypes as the *Da* mutant in its caudal fin. On the other hand, the phenotypes of caudal vertebra and hypural were different between the 2 mutants. This result indicates that this abnormality is caused independently by the decreased expression of *Zic* genes. The targeted disruption of *Hox13* genes results in the anterior transformation or an increased number of caudal vertebrae (Dollé et al., 1993; Economides et al., 2003;

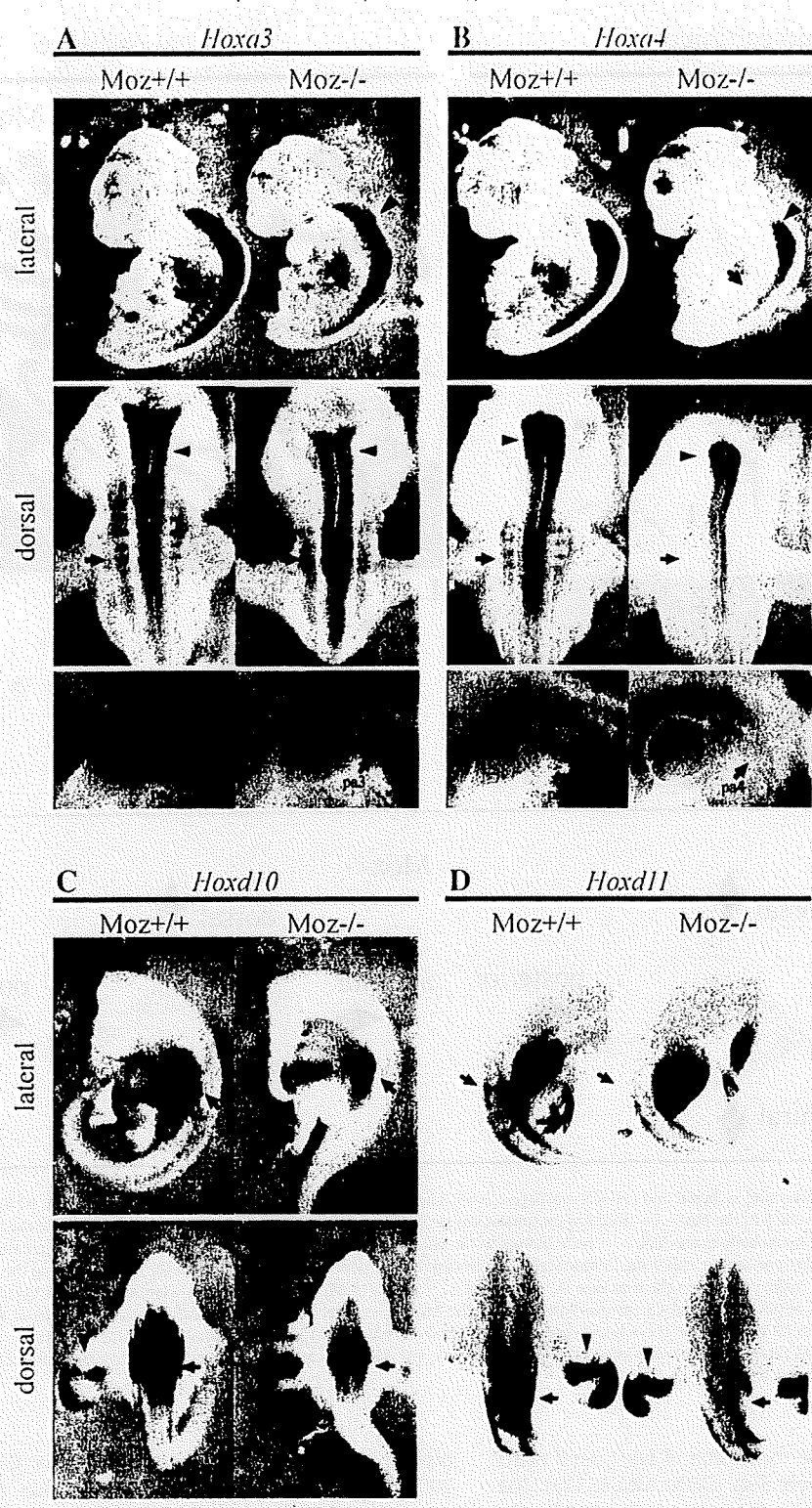

Fig. 10. Moz−/− mice exhibited the decrease of the expression of anterior and posterior *Hox* genes. Whole-mount *in situ* hybridization was performed at E11.5 in the wild type and Moz−/− mice. (A) Expressions of *Hoxa3* in the wild type and Moz−/− mice. Expressions of *Hoxa3* were mildly decreased in the rhombomere and neural tube in Moz−/− mice (arrowheads in upper and middle panels). On the other hand, their expressions were decreased at the somite in Moz−/− mice (arrows in upper and middle panels). Expressions of *Hoxa3* were mildly decreased at the third pharyngeal arch in Moz−/− mice (arrows in lower panels). (B) Expressions of *Hoxa4* in the wild type and Moz−/− mice. A similar decrease was observed in Moz−/− mice (arrows and arrowheads in upper and middle panels). Note that the expressions of *Hoxa4* at the pharyngeal arches were severely decreased in Moz−/− mice (arrows in lower panels). (C) Expressions of *Hoxd10* in the wild type and Moz−/− mice. The expression of the *Hoxd10* was severely decreased in the somite and neural tube (arrows). However the expression of *Hoxd10* in the hind limb was not decreased (arrowheads). (D) Expressions of *Hoxd11* in the wild type and Moz−/− mice. Expressions of *Hoxd11* were also decreased at the somite and neural tube in Moz−/− mice (arrow). Expressions of *Hoxd11* were not affected at the hind limb (arrowhead). pa3; third pharyngeal arch, pa4; fourth pharyngeal arch.

Godwin and Capecchi, 1998). Although an apparent transformation of vertebral morphology was not observed in the *bis* mutant, the hypurals of the caudal vertebrae were reduced in size or disappeared in the *bis* mutant. This phenotype might be caused by the partial transformation of caudal vertebrae into the morphology of anterior ones.

Gene-specific regulation by Brpf1 in the anterior and posterior regions

In this study, we demonstrated that Brpf1 regulates the expression of *Hox* genes in the anterior and posterior regions of the developing body but not that of those in the central region. Previous studies on the function of TrxG mainly were performed on *mll* knock-out mice and focused on the gene-specific regulation of *Hox* genes. In *mll* knock-out mice, the expression of *hoxa7*, *hoxd4*, and *hoxc8* was decreased at the central region of the developing embryo (Glaser et al., 2006; Terranova et al., 2006; Yu et al., 1998, 1995). On the other hand, the *bis* mutant exhibited decreased expression of *Hox* genes in the anterior and posterior regions. It should be noted that the expression of *Hox* genes located at the center of the Hox cluster and expressed in the central region of the developing embryo was not affected or only mildly decreased in the *bis* mutant (Supplementary Fig. 5), implying the gene-specific regulation of Brpf1 in the maintenance of the expression of the *Hox* genes. In A–P axis formation, in addition to *Hox* genes, FGF and RA signals are also involved in the initial establishment of A–P axis formation (Bel-Vialar et al., 2002; Diez del Corral and Storey, 2004). FGF preferentially functions in the anterior and posterior axial formation, whereas RA preferentially functions in the central axial formation. The regions where the expression of *Hox* genes was decreased in the *bis* mutant have a strong relation to the FGF organizing area, suggesting that MOZ HAT complex may collaborate with FGF signaling in the regulation of *Hox* gene expression. In addition, although the expression of *Hox* genes was decreased in various regions of the developing body of the *bis* mutant, the expression of some *Hox* genes was only mildly decreased at certain restricted regions, e.g., hindbrain, posterior pharyngeal arch. These findings suggest that a different requirement for Brpf1 exists at the different regions or that some other factors function redundantly at these regions. To estimate the functional redundancy of Brpf1, we examined the expression of all Brpf families, which include *brpf1*, *brpf2*, and *brpf3*, and found that these genes were expressed in similar regions (data not shown), indicating that *brpf2* and *brpf3* have no functional redundancy in maintaining the Hox expression. In this study, the detailed mechanisms which underlie the maintenance of *Hox* genes have not been clarified. A further study is required to elucidate how the expression of each *Hox* gene in various tissues is differently regulated by the chromatin regulation.

A common role of the MOZ HAT complex in skeletal development via regulating the expression of Hox genes

In this study, we also demonstrated the abnormality of the skeletal patterning in the Moz−/− mice. The shape of the hyoid cartilage was changed in the Moz−/− mice. In the ventral view, the shape of hyoid body was similar to that of Meckel's cartilage. In addition, the accessory process on the greater horn of the hyoid in the Moz−/− mice was similar to the phenotype of *kreisler* mutant mice and zebrafish *valentine* mutant, in which the reduced expression of *Hox3* genes is observed, and the lesser horn of the hyoid is ectopically formed on the greater horn of the hyoid (Frohman et al., 1993; Kimmel et al., 2001; Manzanares et al., 1999; Prince et al., 1998). Consistent with these reports, Moz−/− mice exhibit the reduction of *Hoxa3* transcript at the third pharyngeal arch. In the cervical region, the axis was fused to the exoccipital in the Moz−/− mice. A similar phenotype was demonstrated in the Hox 3 paralogue group knock-out mice (Condie and Capecchi, 1994; Manley and Capecchi, 1997). Furthermore, the neural arch of the C3 had a morphological similarity to that of the axis, and the fused neural arches in cervical vertebrae were similar to those of the *Hoxa4* and *Hoxb4* double knock-out mice (Horan et al., 1995). Consistently, *Hoxa4* transcripts were decreased at the somite in Moz−/− mice, suggesting that the abnormality of cervical vertebrae was caused by A–P axis disruption. Furthermore, in the posterior region, the Moz−/− mice exhibited a decrease of *Hoxd10* and *Hoxd11* expressions. However, we failed to find abnormalities of cartilage formation in the Moz−/− mice at the position of the hind limb (data not shown). It may be possible that finding the abnormality of the Moz−/− mice was difficult, because the posterior skeleton has not fully formed at E14.5. Thus, these results suggest that the abnormal skeletal phenotypes of the Moz−/− mice were caused by the decreased expressions of *Hox* genes, and the common mechanism using MOZ HAT complex exists in the skeletal patterning in vertebrate development.

Acknowledgments

We thank Dr. N. Manley, Dr. M. Araki and Dr. X.J Yang for their kindly gifts of mouse *Hoxa3*, *Hoxa4* and Flag-Moz and HA-Brpf1 plasmid, respectively. We thank Dr. K. Naruse for a gift of the BAC vector, Dr. K. Maruyama for a gift of the α-*globin*-GFP transgenic medaka, Dr. K. Inohaya and Dr. A. Kawakami for many helpful discussions, and finally Dr. I. Kii for reading of manuscript. We also would like to express sincere appreciation to our colleagues for their support during the screening of medaka mutants. We also thank NBRP Medaka for providing a hatching enzyme. This work was supported by grants-in-aid from the Ministry of Education, Culture, Sports, Science, and Technology of Japan.

Appendix A. Supplementary data

Supplementary data associated with this article can be found, in the online version, at doi:10.1016/j.ydbio.2009.02.021.

References

Akasaka, T., Kanno, M., Balling, R., Mieza, M.A., Taniguchi, M., Koseki, H., 1996. A role for mel-18, a Polycomb group-related vertebrate gene, during the anteroposterior specification of the axial skeleton. Development 122, 1513–1522.

Akasaka, T., van Lohuizen, M., van der Lugt, N., Mizutani-Koseki, Y., Kanno, M., Taniguchi, M., Vidal, M., Alkema, M., Berns, A., Koseki, H., 2001. Mice doubly deficient for the polycomb group genes Mel18 and Bmi1 reveal synergy and requirement for maintenance but not initiation of *Hox* gene expression. Development 128, 1587–1597.

Beddington, R.S., Robertson, E.J., 1999. Axis development and early asymmetry in mammals. Cell 96, 195–209.

Bel-Vialar, S., Itasaki, N., Krumlauf, R., 2002. Initiating *Hox* gene expression: in the early chick neural tube differential sensitivity to FGF and RA signaling subdivides the *HoxB* genes in two distinct groups. Development 129, 5103–5115.

Condie, B.G., Capecchi, M.R., 1994. Mice with targeted disruptions in the paralogous genes hoxa-3 and hoxd-3 reveal synergistic interactions. Nature 370, 304–307.

Core, N., Bel, S., Gaunt, S.J., Aurrand-Lions, M., Pearce, J., Fisher, A., Djabali, M., 1997. Altered cellular proliferation and mesoderm patterning in polycomb-M33-deficient mice. Development 124, 721–729.

Crump, J.G., Swartz, M.E., Eberhart, J.K., Kimmel, C.B., 2006. Moz-dependent Hox expression controls segment-specific fate maps of skeletal precursors in the face. Development 133, 2661–2669.

del Mar Lorente, M., Marcos-Gutierrez, C., Perez, C., Schoorlemmer, J., Ramirez, A., Magin, T., Vidal, M., 2000. Loss- and gain-of-function mutations show a polycomb group function for Ring1A in mice. Development 127, 5093–5100.

Deschamps, J., van den Akker, E., Forlani, S., De Graaff, W., Oosterveen, T., Roelen, B., Roelfsema, J., 1999. Initiation, establishment and maintenance of *Hox* gene expression patterns in the mouse. Int. J. Dev. Biol. 43, 635–650.

Deschamps, J., van Nes, J., 2005. Developmental regulation of the *Hox* genes during axial morphogenesis in the mouse. Development 132, 2931–2942.

Dhalluin, C., Carlson, J.E., Zeng, L., He, C., Aggarwal, A.K., Zhou, M.M., 1999. Structure and ligand of a histone acetyltransferase bromodomain. Nature 399, 491–496.

Diez del Corral, R., Storey, K.G., 2004. Opposing FGF and retinoid pathways: a signalling switch that controls differentiation and patterning onset in the extending vertebrate body axis. Bioessays 26, 857–869.

Dolle, P., Dierich, A., LeMeur, M., Schimmang, T., Schuhbaur, B., Chambon, P., Duboule, D., 1993. Disruption of the *Hoxd-13* gene induces localized heterochrony leading to mice with neotenic limbs. Cell 75, 431–441.

Doyon, Y., Cayrou, C., Ullah, M., Landry, A.J., Cote, V., Selleck, W., Lane, W.S., Tan, S., Yang, X.J., Cote, J., 2006. ING tumor suppressor proteins are critical regulators of chromatin acetylation required for genome expression and perpetuation. Mol. Cell 21, 51–64.

Economides, K.D., Zeltser, L., Capecchi, M.R., 2003. Hoxb13 mutations cause overgrowth of caudal spinal cord and tail vertebrae. Dev. Biol. 256, 317–330.

Favier, B., Dolle, P., 1997. Developmental functions of mammalian *Hox* genes. Mol. Hum. Reprod. 3, 115–131.

Frohman, M.A., Martin, G.R., Cordes, S.P., Halamek, L.P., Barsh, G.S., 1993. Altered rhombomere-specific gene expression and hyoid bone differentiation in the mouse segmentation mutant, Kreisler (Kr). Development 117, 925–936.
Gendron-Maguire, M., Mallo, M., Zhang, M., Gridley, T., 1993. Hoxa-2 mutant mice exhibit homeotic transformation of skeletal elements derived from cranial neural crest. Cell 75, 1317–1331.
Glaser, S., Schaft, J., Lubitz, S., Vintersten, K., van der Hoeven, F., Tufteland, K.R., Aasland, R., Anastassiadis, K., Ang, S.L., Stewart, A.F., 2006. Multiple epigenetic maintenance factors implicated by the loss of Mll2 in mouse development. Development 133, 1423–1432.
Godwin, A.R., Capecchi, M.R., 1998. Hoxc13 mutant mice lack external hair. Genes Dev. 12, 11–20.
Hadzhiev, Y., Lele, Z., Schindler, S., Wilson, S.W., Ahlberg, P., Strahle, U., Muller, F., 2007. Hedgehog signaling patterns the outgrowth of unpaired skeletal appendages in zebrafish. BMC Dev. Biol. 7, 75.
Hoegg, S., Boore, J.L., Kuehl, J.V., Meyer, A., 2007. Comparative phylogenomic analyses of teleost fish *Hox* gene clusters: lessons from the cichlid fish *Astatotilapia burtoni*. BMC Genomics 8, 317.
Horan, G.S., Ramirez-Solis, R., Featherstone, M.S., Wolgemuth, D.J., Bradley, A., Behringer, R.R., 1995. Compound mutants for the paralogous hoxa-4, hoxb-4, and hoxd-4 genes show more complete homeotic transformations and a dose-dependent increase in the number of vertebrae transformed. Genes Dev. 9, 1667–1677.
Hunter, M.P., Prince, V.E., 2002. Zebrafish hox paralogue group 2 genes function redundantly as selector genes to pattern the second pharyngeal arch. Dev. Biol. 247, 367–389.
Inohaya, K., Yasumasu, S., Ishimaru, M., Ohyama, A., Iuchi, I., Yamagami, K., 1995. Temporal and spatial patterns of gene expression for the hatching enzyme in the teleost embryo, *Oryzias latipes*. Dev. Biol. 171, 374–385.
Inohaya, K., Yasumasu, S., Yasumasu, I., Iuchi, I., Yamagami, K., 1999. Analysis of the origin and development of hatching gland cells by transplantation of the embryonic shield in the fish, *Oryzias latipes*. Dev. Growth Differ. 41, 557–566.
Iwamatsu, T., 2004. Stages of normal development in the medaka *Oryzias latipes*. Mech. Dev. 121, 605–618.
Izpisua-Belmonte, J.C., Falkenstein, H., Dolle, P., Renucci, A., Duboule, D., 1991. Murine genes related to the *Drosophila* AbdB homeotic genes are sequentially expressed during development of the posterior part of the body. EMBO J. 10, 2279–2289.
Katsumoto, T., Aikawa, Y., Iwama, A., Ueda, S., Ichikawa, H., Ochiya, T., Kitabayashi, I., 2006. MOZ is essential for maintenance of hematopoietic stem cells. Genes Dev. 20, 1321–1330.
Kawazoe, Y., Sekimoto, T., Araki, M., Takagi, K., Araki, K., Yamamura, K., 2002. Region-specific gastrointestinal Hox code during murine embryonal gut development. Dev. Growth Differ. 44, 77–84.
Kimmel, C.B., Miller, C.T., Moens, C.B., 2001. Specification and morphogenesis of the zebrafish larval head skeleton. Dev. Biol. 233, 239–257.
Kimura, T., Jindo, T., Narita, T., Naruse, K., Kobayashi, D., Shin-i, T., Kitagawa, T., Sakaguchi, T., Mitani, H., Shima, A., et al., 2004. Large-scale isolation of ESTs, from medaka embryos and its application to medaka developmental genetics. Mech. Dev. 121, 915–932.
Kmita, M., Duboule, D., 2003. Organizing axes in time and space; 25 years of colinear tinkering. Science 301, 331–333.
Kondo, T., Duboule, D., 1999. Breaking colinearity in the mouse HoxD complex. Cell 97, 407–417.
Kuratani, S., 2005. Developmental studies of the lamprey and hierarchical evolutionary steps towards the acquisition of the jaw. J. Anat. 207, 489–499.
Kurosawa, G., Takamatsu, N., Takahashi, M., Sumitomo, M., Sanaka, E., Yamada, K., Nishii, K., Matsuda, M., Asakawa, S., Ishiguro, H., et al., 2006. Organization and structure of *hox* gene loci in medaka genome and comparison with those of pufferfish and zebrafish genomes. Gene 370, 75–82.
Laue, K., Daujat, S., Crump, J.G., Plaster, N., Roehl, H.H., Kimmel, C.B., Schneider, R., Hammerschmidt, M., 2008. The multidomain protein Brpf1 binds histones and is required for *Hox* gene expression and segmental identity. Development 135, 1935–1946.
Le Douarin, N.M., Jotereau, F.V., 1975. Tracing of cells of the avian thymus through embryonic life in interspecific chimeras. J. Exp. Med. 142, 17–40.
Lewis, E.B., 1978. A gene complex controlling segmentation in *Drosophila*. Nature 276, 565–570.
Lumsden, A., Sprawson, N., Graham, A., 1991. Segmental origin and migration of neural crest cells in the hindbrain region of the chick embryo. Development 113, 1281–1291.
Manley, N.R., Capecchi, M.R., 1995. The role of Hoxa-3 in mouse thymus and thyroid development. Development 121, 1989–2003.
Manley, N.R., Capecchi, M.R., 1997. Hox group 3 paralogous genes act synergistically in the formation of somitic and neural crest-derived structures. Dev. Biol. 192, 274–288.
Manley, N.R., Capecchi, M.R., 1998. Hox group 3 paralogs regulate the development and migration of the thymus, thyroid, and parathyroid glands. Dev. Biol. 195, 1–15.
Manley, N.R., Selleri, L., Brendolan, A., Gordon, J., Cleary, M.L., 2004. Abnormalities of caudal pharyngeal pouch development in Pbx1 knockout mice mimic loss of Hox3 paralogs. Dev. Biol. 276, 301–312.
Manzanares, M., Trainor, P.A., Nonchev, S., Ariza-McNaughton, L., Brodie, J., Gould, A., Marshall, H., Morrison, A., Kwan, C.T., Sham, M.H., et al., 1999. The role of kreisler in segmentation during hindbrain development. Dev. Biol. 211, 220–237.
Miller, C.T., Maves, L., Kimmel, C.B., 2004. moz regulates Hox expression and pharyngeal segmental identity in zebrafish. Development 131, 2443–2461.
Moens, C.B., Cordes, S.P., Giorgianni, M.W., Barsh, G.S., Kimmel, C.B., 1998. Equivalence in the genetic control of hindbrain segmentation in fish and mouse. Development 125, 381–391.
Mullins, M.C., Hammerschmidt, M., Haffter, P., Nusslein-Volhard, C., 1994. Large-scale mutagenesis in the zebrafish: in search of genes controlling development in a vertebrate. Curr. Biol. 4, 189–202.
Naruse, K., Fukamachi, S., Mitani, H., Kondo, M., Matsuoka, T., Kondo, S., Hanamura, N., Morita, Y., Hasegawa, K., Nishigaki, R., et al., 2000. A detailed linkage map of medaka, *Oryzias latipes*: comparative genomics and genome evolution. Genetics 154, 1773–1784.
Noden, D.M., 1978. The control of avian cephalic neural crest cytodifferentiation. I. Skeletal and connective tissues. Dev. Biol. 67, 296–312.
Noden, D.M., 1988. Interactions and fates of avian craniofacial mesenchyme. Development 103, 121–140 Suppl.
Ohtsuka, M., Kikuchi, N., Yokoi, H., Kinoshita, M., Wakamatsu, Y., Ozato, K., Takeda, H., Inoko, H., Kimura, M., 2004. Possible roles of zic1 and zic4, identified within the medaka Double anal fin (Da) locus, in dorsoventral patterning of the trunk-tail region related to phenotypes of the Da mutant. Mech. Dev. 121, 873–882.
Papp, B., Muller, J., 2006. Histone trimethylation and the maintenance of transcriptional ON and OFF states by trxG and PcG proteins. Genes Dev. 20, 2041–2054.
Pena, P.V., Davrazou, F., Shi, X., Walter, K.L., Verkhusha, V.V., Gozani, O., Zhao, R., Kutateladze, T.G., 2006. Molecular mechanism of histone H3K4me3 recognition by plant homeodomain of ING2. Nature 442, 100–103.
Piotrowski, T., Nusslein-Volhard, C., 2000. The endoderm plays an important role in patterning the segmented pharyngeal region in zebrafish (*Danio rerio*). Dev. Biol. 225, 339–356.
Prince, V.E., Moens, C.B., Kimmel, C.B., Ho, R.K., 1998. Zebrafish *hox* genes: expression in the hindbrain region of wild-type and mutants of the segmentation gene, *valentino*. Development 125, 393–406.
Rancourt, D.E., Tsuzuki, T., Capecchi, M.R., 1995. Genetic interaction between hoxb-5 and hoxb-6 is revealed by nonallelic noncomplementation. Genes Dev. 9, 108–122.
Renucci, A., Zappavigna, V., Zakany, J., Izpisua-Belmonte, J.C., Burki, K., Duboule, D., 1992. Comparison of mouse and human HOX-4 complexes defines conserved sequences involved in the regulation of Hox-4.4. EMBO J. 11, 1459–1468.
Rinn, J.L., Wang, J.K., Allen, N., Brugmann, S.A., Mikels, A.J., Liu, H., Ridky, T.W., Stadler, H.S., Nusse, R., Helms, J.A., et al., 2008. A dermal HOX transcriptional program regulates site-specific epidermal fate. Genes Dev. 22, 303–307.
Rivera-Perez, J.A., Mallo, M., Gendron-Maguire, M., Gridley, T., Behringer, R.R., 1995. Goosecoid is not an essential component of the mouse gastrula organizer but is required for craniofacial and rib development. Development 121, 3005–3012.
Rokudai, S., Aikawa, Y., Tagata, Y., Tsuchida, N., Taya, Y., Kitabayashi, I., 2009. Monocytic leukemia zinc finger (MOZ) interacts with p53 to induce p21 expression and cell-cycle arrest. J. Biol. Chem. 284, 237–244.
Sakaguchi, S., Nakatani, Y., Takamatsu, N., Hori, H., Kawakami, A., Inohaya, K., Kudo, A., 2006. Medaka unextended-fin mutants suggest a role for HoxbBa in cell migration and osteoblast differentiation during appendage formation. Dev. Biol. 293, 426–438.
Santagati, F., Minoux, M., Ren, S.Y., Rijli, F.M., 2005. Temporal requirement of Hoxa2 in cranial neural crest skeletal morphogenesis. Development 132, 4927–4936.
Solnica-Krezel, L., Schier, A.F., Driever, W., 1994. Efficient recovery of ENU-induced mutations from the zebrafish germline. Genetics 136, 1401–1420.
Soshnikova, N., Duboule, D., 2008. Epigenetic regulation of *Hox* gene activation: the waltz of methyls. Bioessays 30, 199–202.
Suzuki, M., Mizutani-Koseki, Y., Fujimura, Y., Miyagishima, H., Kaneko, T., Takada, Y., Akasaka, T., Tanzawa, H., Takihara, Y., Nakano, M., et al., 2002. Involvement of the Polycomb-group gene Ring1B in the specification of the anterior–posterior axis in mice. Development 129, 4171–4183.
Takihara, Y., Tomotsune, D., Shirai, M., Katoh-Fukui, Y., Nishii, K., Motaleb, M.A., Nomura, M., Tsuchiya, R., Fujita, Y., Shibata, Y., et al., 1997. Targeted disruption of the mouse homologue of the *Drosophila* polyhomeotic gene leads to altered anteroposterior patterning and neural crest defects. Development 124, 3673–3682.
Tanaka, K., Ohisa, S., Orihara, N., Sakaguchi, S., Horie, K., Hibiya, K., Konno, S., Miyake, A., Setiamarga, D., Takeda, H., et al., 2004. Characterization of mutations affecting embryonic hematopoiesis in the medaka, *Oryzias latipes*. Mech. Dev. 121, 739–746.
Taverna, S.D., Ilin, S., Rogers, R.S., Tanny, J.C., Lavender, H., Li, H., Baker, L., Boyle, J., Blair, L.P., Chait, B.T., et al., 2006. Yng1 PHD finger binding to H3 trimethylated at K4 promotes NuA3 HAT activity at K14 of H3 and transcription at a subset of targeted ORFs. Mol. Cell 24, 785–796.
Terranova, R., Agherbi, H., Boned, A., Meresse, S., Djabali, M., 2006. Histone and DNA methylation defects at *Hox* genes in mice expressing a SET domain-truncated form of Mll. Proc. Natl. Acad. Sci. U. S. A. 103, 6629–6634.
Thermes, V., Grabher, C., Ristoratore, F., Bourrat, F., Choulika, A., Wittbrodt, J., Joly, J.S., 2002. I-SceI meganuclease mediates highly efficient transgenesis in fish. Mech. Dev. 118, 91–98.
Thomas, T., Corcoran, L.M., Gugasyan, R., Dixon, M.P., Brodnicki, T., Nutt, S.L., Metcalf, D., Voss, A.K., 2006. Monocytic leukemia zinc finger protein is essential for the development of long-term reconstituting hematopoietic stem cells. Genes Dev. 20, 1175–1186.
Tucker, A.S., Watson, R.P., Lettice, L.A., Yamada, G., Hill, R.E., 2004. Bapx1 regulates patterning in the middle ear: altered regulatory role in the transition from the proximal jaw during vertebrate evolution. Development 131, 1235–1245.
Turlure, F., Maertens, G., Rahman, S., Cherepanov, P., Engelman, A., 2006. A tripartite DNA-binding element, comprised of the nuclear localization signal and two AT-hook motifs, mediates the association of LEDGF/p75 with chromatin in vivo. Nucleic Acids Res. 34, 1653–1675.
Ullah, M., Pelletier, N., Xiao, L., Zhao, S.P., Wang, K., Degerny, C., Tahmasebi, S., Cayrou, C., Doyon, Y., Goh, S.L., et al., 2008. Molecular architecture of quartet MOZ/MORF histone acetyltransferase complexes. Mol. Cell. Biol. 28, 6828–6843.
van Eeden, F.J., Granato, M., Odenthal, J., Haffter, P., 1999. Developmental mutant screens in the zebrafish. Methods Cell. Biol. 60, 21–41.